Supercritical drying of cementitious materials

Zhidong Zhang, George W Scherer

Supercritical drying of cementitious materials

Zhidong Zhang, George W. Scherer*

[a]Department of Civil and Environmental Engineering, Princeton University, Princeton, NJ 08544, USA

Abstract

Techniques to characterize the microstructure of hydrated cement require dried materials. However, the microstructure of hydrated products is significantly altered by high capillary forces during drying when using the conventional drying methods. To avoid drying stresses when preparing samples, we have employed supercritical drying (SCD) which has been used for decades to prepare aerogels that undergo no shrinkage during drying, but has rarely been used for cementitious materials. The pore solution is first replaced with isopropanol, and then with trifluoromethane (R23). The temperature and pressure are raised above the critical point, where no menisci or capillary pressure can exist; therefore, the dried samples are free of artifacts created by stresses. Images from scanning electron microscope show less compact morphology for supercritically dried samples than that dried by conventional methods, while BET surface areas of SCD samples are very close to samples dried by isopropanol replacement method. This can be explained by the fact that isopropanol and supercritical fluid enter the micropores and block them. The nature of the chemical interactions of isopropanol and R23 with cement pastes are still not clear, but no reaction products were identified in the present study.

Keywords: supercritical drying (E), microstructure (C), trifluoromethane (C), isopropanol exchange (A), scanning electron microscopy (B), nitrogen adsorption (A)

1. Introduction

Pore structure of cementitious materials is a decisive factor that can be used to determine materials properties, such as permeability, and also can help us to understand the process of nucleation and growth of hydration products. To characterize the pore structure and the morphology of calcium silicate hydrate (C-S-H), various techniques have been used, such as scanning electron microscopy (SEM), mercury intrusion porosimetry (MIP), gas (nitrogen or water vapor) adsorption, etc. These techniques require dried samples, and unfortunately the pore structure is significantly affected by drying.

Drying can remove water, classified as evaporable water, from two types of pores. Capillary pores are larger and hold water in saturated conditions but lose water on exposure to air (at ambient relative humidity). Gel pores are nanometer-size pores (< 10 nm) [1] and water present in gel pores is more strongly bound than capillary water, so that ambient relative humidity (RH) may not be able to remove; reduced pressure or elevated temperature is required. No matter what drying method is used, the ideal condition is that no water is left in capillary and gel pores after drying. The residual evaporable water in the material interferes with the characterization of the pore structure. However, in most drying methods, the interface between liquid water and air creates capillary pressure. According to the Young-Kelvin equation, capillary pressure increases with the decrease of pore size ($P_c \propto 1/r$). This means that the removal of gel-pore water can cause high capillary pressure so the damage to gel pores is more significant than that to capillary pores. The damage is mainly from the shrinkage of pores and rearrangement of particles. Various drying methods used to minimize the influence of drying on the pore structure have been extensively reviewed in the literature [2, 3].

The process of taking water out the porous media can be achieved in three ways according to the phases of water (Fig. 1). Direct drying (e.g., flowing N_2 drying, oven drying and vacuum drying) lets liquid water directly evaporate to the vapor phase. The vapor pressure of water is at the saturation level at the surface of the body, and the rate

*Corresponding author. Tel.: +1 609 258 5680; fax: +1 609 258 1563. E-mail address:scherer@princeton.edu(G.W. Scherer).

of evaporation is controlled by diffusion through a boundary layer [4, 5]. The flowing N_2 creates the zero-humidity environment to force liquid water to evaporate, and the higher the velocity of the nitrogen, the thinner the boundary layer, which accelerates the kinetics of drying. Oven drying, either at 60 °C or 105 °C, speeds up the evaporation by raising the vapor pressure and diffusivity of the water vapor, but usually does not permit strong convection. Oven-drying above 40 °C may lead to dehydration and rearrangement of hydration products [6], and consequently more coarsening of pore structure than other methods. Vacuum drying is also an acceleration process which decreases the surrounding vapor pressure, but it is slow because the absence of convection results in a thick boundary layer. Direct drying methods do not eliminate or reduce capillary pressure (except for the small effect of temperature on surface tension), so materials still suffer high capillary forces.

Capillary pressure can be reduced by replacing water with low-surface-tension solvents. Solvent replacement drying is considered as the best technique with respect to preservation of the pore structure [7, 3]. Commonly used solvents, such as acetone, ethanol, isopropanol, methanol, tetrahydrofuran and dimethyl sulfoxide, are miscible with water. When samples are immersed in the solvent, the interdiffusion of water and solvent reduces water content with time. Hydration can be arrested in a short time by reducing the water activity in the cement matrix [8] while it may take a long time to completely replace water, depending on solvent diffusion coefficient, sample size, etc. After solvent replacement, samples can be subjected to normal drying methods, either low RH drying or oven drying or vacuum drying. Due to the low surface tension, drying of solvent creates much smaller capillary pressure, so that solvent exchange presumably causes less damage to the microstructure than water. The main risk from this method is that some solvents can react with cementitious materials. For instance, thermogravimetric analysis (TGA) results from both cement paste and calcium hydroxide showed that methanol alters sample composition by reacting to form a carbonate-like product [9]. Various techniques, such as X-ray diffraction (XRD), infrared spectroscopy, thermal analysis and conduction calorimetry, further show that when methanol is mixed with calcium hydroxide, methylated complex or calcium methoxide is formed [10]. The reaction of acetone with calcium hydroxide was also found to affect TGA results because of aldol condensation [11]. Dimensional changes are observed for the samples immersed in acetone, ethanol and isopropanol. Beaudoin [10] argued this is the sign of chemical interaction between solvent and calcium hydroxide, although no reaction products were identified. Zhang and Scherer compared solvent exchange by using isopropanol, tetrahydrofuran, ethanol and acetone. The TGA curve for isopropanol (IPA) had less weight loss between 600 °C and 1000 °C than other solvents. Weight loss during this temperature range may indicate chemical reaction or strong absorption between solvents and hydration products. They concluded that solvent exchange with isopropanol can best preserve the microstructure.

If one wants to eliminate capillary pressure during drying, freeze-drying is one of the choices. When samples are directly immersed in liquid nitrogen, pore water is instantaneously frozen, so hydration stops simultaneously. Then, ice is sublimated under vacuum without going through the liquid state. Freeze-drying is considered as the best way to chemically preserve each component in cementitious materials. However, the freezing of water in the pore network generates the crystallization pressure that can damage the microstructure of hydration products [12]. As we know, when water is frozen into ice, the volume rises about 10%. The volume expansion also creates pressure from the solid body and can cause damage similar to oven drying [13, 14]. Another drawback is that freeze-drying needs long time for sublimation and removes less water compared to other methods [13].

The question still remains as to which one is the best drying method in terms of preserving the microstructure of hydration products. Various techniques have been used by researchers in the literature to quantify different drying methods. By using MIP, Galle [13] recommended freeze-drying as the best method to investigate the pore structure of cement based materials. This recommendation was supported by Korpa and Trettin[15] who concluded that freeze-drying gives the most accurate picture for the microstructure based on data measured by nitrogen adsorption (NAD), TGA and Nuclear Magnetic Resonance spectroscopy (NMR). However, using the same techniques, Feldman and Beaudoin [16] concluded that isopropanol exchange was less destructive than vacuum drying and drying at low RH. Konecny and Naqvi [7] concluded that solvent replacement with isopropanol was preferable for MIP samples. By analyzing the water vapor sorption isotherms measured by Dynamic Vapor Sorption (DVS), Snoeck et al. [17] reported that vacuum-drying and the solvent exchange with isopropanol can minimize the effect on the microstructure during drying the cementitious samples. Clearly, the results are contradictory, but a thorough review of the literature concluded that solvent exchange with isopropanol is the best method to preserve the microstructure [3].

The purpose of solvent exchange is to reduce surface tension and thereby reduce the capillary pressure. There is

one method that can eliminate capillary pressure entirely. It is known as supercritical drying (SCD) or critical point drying, which has been mentioned in the literature but rarely used to dry cementitious materials [2, 3]. In this method, the temperature and pressure are raised above the critical point of the pore liquid (see Fig. 1), following a path such that the liquid becomes a supercritical fluid without creating a liquid-gas interface, so no capillary pressure develops in the pores [18]. Supercritical fluid can be removed by depressurization while the temperature remains above the critical temperature. This technique has been widely used to make aerogels that have high porosity (typically > 95%) and fragile pore structure [19]. To avoid the high critical temperature of water, it is common to exchange the pore liquid with a fluid that has a lower critical point, most commonly carbon dioxide (CO_2 , critical point at 31.03 °C and 7.38 MPa).

The most challenging problem for supercritical drying of cementitious materials is to find a suitable supercritical fluid. In the study by Litvan [20], samples were first washed with methanol, followed by exchange with pentane (critical point 196.7 °C, 3.36 MPa). The final step was to evaporate pentane above the critical pressure and temperature (which was done at 205 °C). There are two obvious risks that can potentially alter microstructure in his study. First, the critical temperature for pentane is high enough to dehydrate C-S-H and ettringite. Second, methanol can react with calcium hydroxide as stated above. Using carbon dioxide would solve the first risk, but also carbonate the C-S-H, as well as calcium hydroxide. The ideal fluid should have minimal chemical reaction with cement and hydration products, and have a critical point below 40 °C.

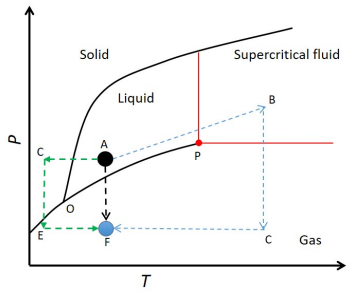

Figure 1: An example of phase diagram.

Freon® R23 (CHF_3) has been suggested for supercritical drying of cementitious materials because it has a low critical point (25.7 °C and 4.82 MPa) and is expected to be inert to cement [3]. This paper is devoted to examining the use of R23 as supercritical fluid to dry cementitious materials. We focus on drying of pastes hydrated for 24 hours or less, to investigate the microstructure when it is most fragile.

2. Overview of supercritical drying

Because R23 is nonpolar, it is immiscible with water, so an intermediate is needed. A solvent can be used due to the good immiscibility with both water and R23. As concluded in the literature, isopropanol is the best solvent for cementitious materials, and it is used in this study. The main steps to perform supercritical drying are: firstly to replace water by isopropanol, then to replace isopropanol by R23 exchange, and lastly to pressurize and heat R23 to supercritical fluid and vent it (see Fig. 2). At ambient pressure and temperature, R23 is gas, but exchange with isopropanol must be done in the liquid state, so an autoclave is required for the steps involving R23.

In the following parts of this paper, we will go through all these steps and investigate the potential issues. Characterization techniques, such as scanning electron microscopy and nitrogen adsorption, are used to assess whether supercritical drying can better preserve the microstructure than other drying methods.

3. Isopropanol exchange

Isopropanol has been recognized as the preferred solvent to dry cementitious materials [3], but there are insufficient data in the literature to predict the rate of exchange. The time to exchange pore water with isopropanol depends on

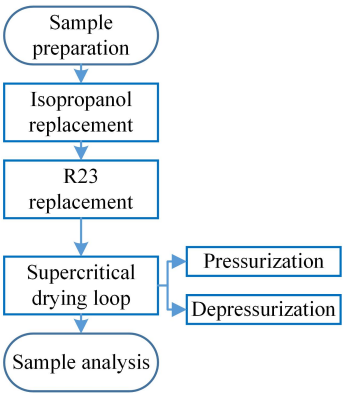

Figure 2: The main steps for supercritical drying.

several factors, such as porosity, pore size, size of the specimen, and the interdiffusion coefficient (assuming that isopropanol/water exchange is a pure diffusion process). For a given water-to-cement ratio (w/c), porosity and pore size generally decrease as the hydration age increases. The only unknown is the diffusion coefficient. Feldman [16] measured the diffusivity in very mature paste with various w/c, and found values on the order of 5 $\times 10^{-12}$ m^2/s. Parrott [21] reported exchange times for alite pastes, but did not extract diffusivities. He did, however, show that the diffusivity is proportional to the viscosity of the solvent, as expected from the Stokes-Einstein equation. Zhang and Scherer used an approximate value of 1×10^{-11} m^2/s in their study [3]. They also analyzed data measured by Gran and Hansen for 3-year old cement paste [22] and estimated a diffusion coefficient of 3×10^{-12} m^2/s for paste with w/c = 0.3, and 3×10^{-11} m^2/s for paste with w/c = 1.0. However, there are no data available for paste at the early age that we will use for the present supercritical drying experiments.

In this study, we carried out isopropanol/water exchange tests to determine the interdiffusion coefficient. Type I ordinary Portland cement with w/c = 0.5 (by mass) was used. After adding deionized water into cement, the material was hand mixed for 1 minute and then mixed by a vortex mixer (Stuart Vortex Mixers SA8) for additional 3 minutes. The paste was cast in a plastic pipette with 6 mm internal diameter. After about 20 hours curing, the cylindrical paste was removed from the pipette and stored in lime water until testing. The specimen used for the test is about 8 cm in length. Prior to the test, the diameter was measured, which ranged from 5.7 to 5.9 cm. When the specimen was just taken out lime water, water on the surface was gently removed by lab tissues and then it was hung under a balance and slowly dipped in isopropanol until it was totally immersed. The mass change was recorded immediately after the specimen was immersed in isopropanol. Specimens cured for 1, 3, 7, and 14 days were tested. The density of isopropanol is smaller than that of water, so the mass of the specimen decreases as isopropanol gradually diffuses into the material. The porosity was determined by the mass difference between the saturated state and the dried state in a 60 °C oven.

During the exchange, water diffuses into the material as isopropanol diffuses out. Fick's second law is used to describe the mutual diffusion process. Since relatively long cylindrical specimens (length/diameter > 10) were employed for the exchange measurements, we only consider the radial diffusion and the effect of the two ends (whose area is < 4% of that of the lateral surface) is neglected.

$$\frac{\partial C}{\partial t} = \frac{1}{r}\frac{\partial}{\partial r}\left[rD_{WI}(C)\frac{\partial C}{\partial r}\right] \tag{1}$$

where C is the normalized isopropanol concentration and D_{WI} is the mutual diffusion coefficient. In a porous medium such as hydrated cement paste, the effective diffusion coefficient depends on the porosity ϕ and tortuosity τ [23].

$$D_{WI} = \frac{\phi}{\tau}D^0_{WI} \tag{2}$$

where D^0_{WI} is the bulk diffusion coefficient between water and isopropanol. Since there are no suitable data found in the literature, the Stokes-Einstein equation is used to determine D^0_{WI}.

$$D^0_{WI} = \frac{k_B T}{\alpha \pi \eta_{WI} R_{WI}} \tag{3}$$

where $k_B = 1.38 \times 10^{-23}$ is Boltzmann constant and T (K) is the temperature. The average molecule radius of the system R_{WI} (m) is calculated based on the mole fraction of each component in the system, by using radii of water (0.15 nm) and IPA (0.25 nm). η_{WI} (Pa/s) is the dynamic viscosity of the mixture and has been measured in the literature [24] as a function of isopropanol mole fraction. The constant α is typically in the range of 4 - 6, where 6 is used for the case that very large particles diffuse into the system with small particles, and for the system with close molecule size, α is smaller (4 is suggested in [25, 26]). Based on the measured water self-diffusion coefficient (2.5×10^{-9} m^2/s [27]), α can be calculated from Eq. (3) and is found to be 4.2, which is very close to the value suggested in the literature.

The value of D^0_{WI} calculated from Eq. (3) is shown in Fig. 3. The self-diffusion coefficients for water and isopropanol match very well with data reported in the literature (0.6×10^{-9} m^2/s [28] for isopropanol). The curve in Figure 3 is different from the one measured by Pratt and Wakeham [29] who reported that D^0_{WI} peaks at isopropanol mole fraction = 0.8. Their data are dubious, owing to the odd shape of the curve and the erroneous value they report for pure water. The measured viscosity does not show any peak so their data are not used in the present study.

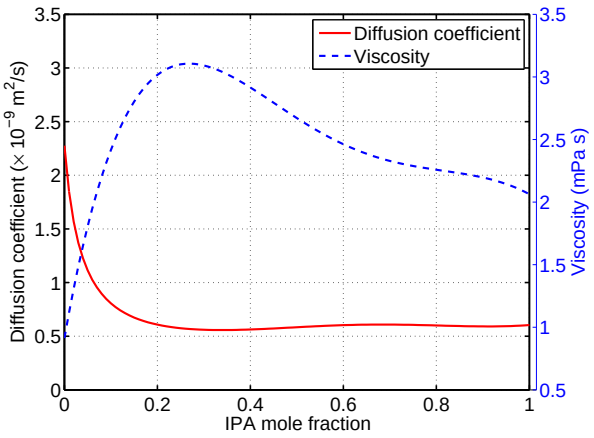

Figure 3: Bulk diffusion coefficient D^0_{WI} during IPA/water exchange. Viscosity data are taken from [24]

In Eqs. (2) and (3), the only unknown is the tortuosity τ, which can be determined by fitting the measured mass loss curve during the isopropanol-water exchange. The measured and fitted mass loss curves are shown in Fig. 4. For 1, 7 and 14-d specimens, the fits are very good, except for the 3-d specimen. The most likely reason is that microcracks are developing during the exchange (see the Section 8.1).

The averaged diffusion coefficients are provided in Table 1 for different samples at different ages. They are around 1×10^{-11} m^2/s which is in agreement with the value estimated by Zhang and Scherer [3].

Table 1: Porosity and diffusion coefficient for cement pastes at different ages.

Age (d)	1	3	7	14
Porosity	0.445	0.442	0.398	0.388
Averaged D_{WI} ($\times10^{-11}$ m^2/s)	1.84	1.3	0.97	0.92
Tortuosity	56	70	94	97

Accordingly, the exchange duration for different sizes and ages of specimens can be calculated. If the exchange criterion is set as 99.9% water in the specimen replaced by isopropanol, the calculated duration is shown in Fig. 5 for two types of sample geometry, sphere and plate. For larger and older specimens, exchange duration is much longer. This encourages us to use specimens as small as possible to reduce the exchange time.

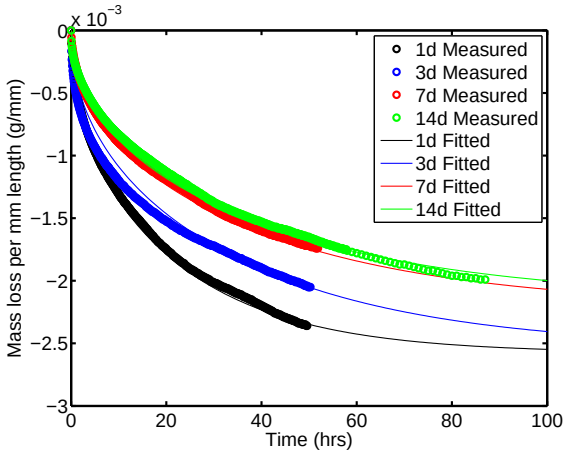

Figure 4: Measured and calculated mass change during isopropanol/water exchange at different ages.

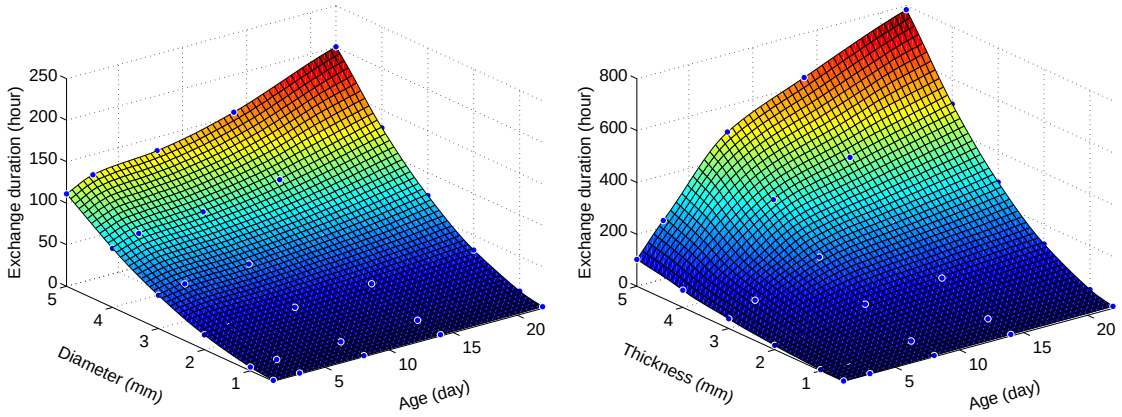

(a) Sphere (b) Plate

Figure 5: Calculated exchange duration for OPC specimens with different size at different ages (w/c=0.5). Dots are calculated results by using diffusion model based on the measured diffusion coefficient. For plate specimen, we assume that exchange only occurs from one side and the other side is isolated.

4. Supercritical fluid exchange

In this step, isopropanol must be replaced by R23 so that the supercritical drying can be accomplished. This exchange is analogous to the exchange between isopropanol and water, meaning that it is considered as a pure diffusion process and the diffusion coefficient is needed. Again, the Stokes-Einstein equation is used here.

$$D_{IR} = \frac{\phi}{\tau} D^0_{IR} = \frac{\phi}{\tau} \frac{k_B T}{\alpha \pi \eta_{IR} R_{IR}} \tag{4}$$

where the subscript IR represents the isopropanol/R23 mixture. Other symbols have the same meanings as in Eq. (2).

The tortuosity τ has been determined in the previous section for cement pastes at different ages. The radius of the R23 molecule, 0.2 nm [30], is used to calculate the average molecular radius R_{IR} of the isopropanol/R23 mixture. Hence, the only unknown in Eq. (4) is the viscosity η_{IR} of the mixture.

At room temperature and atmospheric pressure, R23 is gas, which can not be directly used for exchange, so it must be pressurized into the liquid state. Here, we choose to perform exchange at 5MPa (above the vapor-liquid equilibrium pressure) and at 25 °C (below the critical temperature). However, no studies on the mixture of isopropanol/R23 can be

found in the literature so we will calculate the mixture's viscosity using a UNIFAC-type equation that has been found widely applicable with reasonable accuracies for binary mixtures with alcohols [31, 32], especially for those having similar molecule size [33]:

$$\ln(\eta_{IR}V_{IR}) = \sum_{i=1}^{2} x_i \ln(\eta_i V_i) + \frac{\Delta G_E^*}{RT} \tag{5}$$

where M_{IR} is the molar volume of the isopropanol/R23 mixture. The subscript i represents either isopropanol or R23. x is the mole fraction of each component. ΔG_E^* (J/mol) is the excess Gibbs free energy of activation for viscous flow.

To determine η_{IR}, viscosities of the pure liquids must be known. Yokoyama and Takahashi [34] used an oscillating-disk viscometer to measure gaseous viscosity of R23, but temperature is only up to 30 °C and pressure is up to 5.66 MPa, which are not exactly in the range for our experiments (temperature 25 - 40 °C and pressure up to 8 MPa). Shan et al. [35] have applied the modified reaction rate theory to R23 for the calculation of viscosity in the supercritical and liquid regions (temperature up to 300 °C and pressure up to 60 MPa). Coparison of visicosity at 25 °C and 5 MPa, two studies provided very close data so that we take viscosities from the latter paper for calculations. Tanaka et al. [36] measured the viscosity of liquid isopropanol at different pressures by using a falling-cylinder viscometer. These measured data are provided in Table 2.

Table 2: Measured viscosities of R23 [35] and isopropanol [36] (Unit: Pa·s).

Pressure	R23		Isopropanol	
(MPa)	25 °C	40 °C	25 °C	40 °C
5	0.053	0.020	2.147	1.487
6	0.064	0.025	2.081	1.442
7	0.070	0.041	2.093	1.450

The only unknown in Eq. (5) is ΔG_E^* which is related to molecular geometry and the interaction between the functional groups of the molecules involved. Again, there are no data about excess Gibbs free energy of activation for isopropanol/R23 mixture in the literature. If we know one measured viscosity value for the mixture at a given pressure, ΔG_E^* can be determined and thus the entire viscosity curve can be calculated. Here, we adopt the dynamic pressurization method which was developed to measure the permeability of porous media by Gross and Scherer [37]. In this method, a silica gel with high porosity was used and all properties were accurately given in [37]. By performing a dynamic pressurization experiment on a silica gel, as in [37], we were able to find the viscosity of the R23/IPA mixture. A detailed description of this method is provided in AppendixA. By fitting the measured pressure *vs.* strain curve (isopropanol mole friction $x_I = 0.3$), the values for viscosity at different pressures are given in Table 3. The values of fitted ΔG_E^* are also given in Table 3. The negative values are associated with the existence of weak interaction between two components [38, 39].

Table 3: Viscosity of isopropanol/R23 mixtures measured by dynamic pressurization ($x_I = 0.3$).

Pressure (MPa)	Viscosity η_{IR} (mPa·s)	G_E^* (J/mole)
5	0.140	-950
6	0.158	-985
7	0.175	-905

The calculated viscosity and diffusion coefficient curves are shown in Fig. 6. Pressure has very limited effect on the viscosity curve as well as the diffusion coefficient. The calculated self-diffusion coefficient for R23 is above 45 $\times 10^{-9} m^2/s$ which is about twenty times higher than the self-diffusion coefficient of water shown in Fig. 3. Measured self-diffusion coefficients for R23 are only found in the studies by Prielmeier et al. [30]. They employed a modified high resolution NMR spectrometer to determine the self-diffusion coefficient between 142 K and 250 K at various pressures. By interpolating the measured data at saturation pressure, we find that the self-diffusion coefficient is about 15 $\times 10^{-9} m^2/s$ at 25 °C and 4.7 MPa. This value is lower than that shown in Fig. 6, but still about 6 times higher than water. Hence, the isopropanol/R23 exchange can be completed in a much shorter duration than the exchange of water/isopropanol.

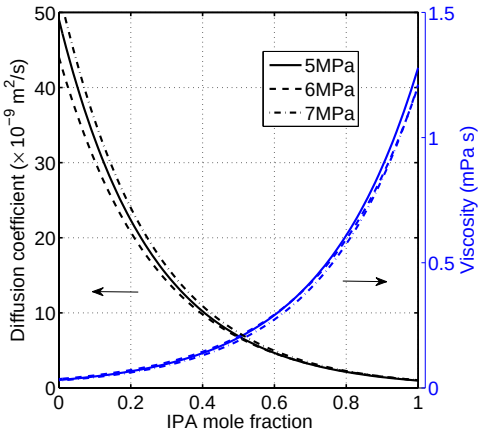

Figure 6: Calculated bulk diffusion coefficient D^0_{IR} and viscosity η_{IR} curves for isopropanol/R23 exchange.

5. Pressure control

In the next step, the specimen is subjected to the pressure loop, including pressurization and depressurization.

5.1. Pressurization

The purpose of this step is to pressurize and heat the liquid R23 above the critical point. In general, pressurization does not have a significant impact on cementitious materials because they have higher compressive strength than tensile strength, and compared to compressive strength, pressure for SCD is relatively low (e.g. [40]), so materials can resist the force caused by the compression of the liquid. Nevertheless, to minimize the risk of damage, two factors are considered in this study. One is the expansion of liquid due to the heating [41], because expansion of the pore liquid creates tensile stress in the network, while pressure increases with heating; thus, the heating rate should be consistent with the pressure rising rate. This can also minimize the effect of another factor - the change of liquid density. If a density gradient is established between the interior and surface of the specimen, flow of liquid will occur due to the gravity and diffusion. This factor has less opportunity to cause damage, but it is considered by the present study.

Both factors can be avoided if during pressurization, (1) the liquid density is kept nearly the same in the interior and exterior of the material, and (2) the pressurization curve follows the temperature/pressure path by using the equation of state of pure R23 [42]. The pressurization curve that ensures the constant liquid density during pressurization, is shown in Fig. 7. The exchange condition is set at 5 MPa and 25 °C, and the corresponding R23 density is about 780 g/ml which is very close the density of isopropanol (781 g/ml) at the same state. In the following pressurization step, the density of R23 is controlled to be the same as the density of isopropanol.

5.2. Depressurization

This step is the most challenging part for supercritical drying, because it involves a huge volume expansion when pressure is decreasing. As the pressure in the autoclave drops, the fluid in the pores expands and flows out of the body. The depressurization rate must be slow enough to allow the fluid to leave the body as it expands, rather than expanding within the pores and creating tensile stress in the solid phase [43]. Cementitious materials are more sensitive to depressurization than to pressurization because of their relatively low tensile strength. If the tensile stress is higher than the tensile strength of the material, damage will occurs; therefore, the depressurization rate must be carefully controlled.

The pressure-induced stresses in the porous body have been analyzed by Scherer [41, 43], Scherer et al. [44] and Gross and Scherer [37]. Those analyzes applied to gels, in which the stiffness of the solid network is small compared to the bulk modulus of the fluid. In cementitious materials, the network is relatively stiff, so the analysis has to be modified. The details are presented in the Supplementary material. If the pressure in the autoclave, P_A, drops too quickly, there will be a strong gradient in the density of the fluid, ρ_F, and possibly damaging stresses will

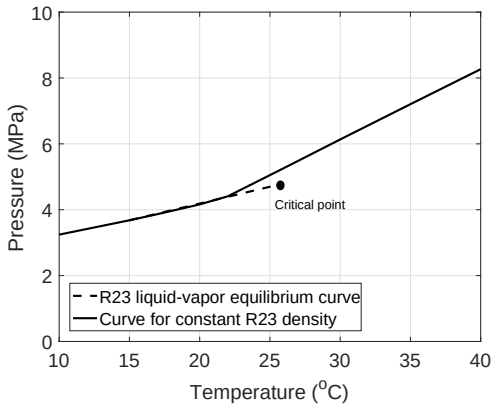

Figure 7: Controlled R23 density during pressurization.

result. Therefore, we are interested in the case where such gradients are small, which means that ρ_F can be removed from within the spatial derivatives in the continuity equation. As shown in the Supplement, with this assumption, the continuity equation for a planar sample drying from both sides ($u = 0$ and $u = 1$) can be written as

$$\left(\frac{b-\phi}{K_s}+\frac{b^2\beta}{K_p}\right)\dot{P}=\frac{k}{\eta L^2}\frac{\partial^2 P}{\partial u^2}-\left(\frac{b^2(1-\beta)}{K_p}+\frac{\phi}{\rho_F}\frac{\partial\rho_F}{\partial\langle P\rangle}\right)\left\langle\dot{P}\right\rangle+\frac{b\dot{P}_A}{K_p} \tag{6}$$

where $b = 1 - K_p/K_s$ is the Biot coefficient, $\beta = (1 + \nu_p)/[3(1 - \nu_p)]$, ν_p is Poisson's ratio of the porous network, η is the viscosity of pore fluid, k is the permeability (m^2), P is the fluid pressure in the pore network, K_p and K_s are bulk modulus of the pore network and solid phase, respectively. The angle brackets represent the volumetric average. The superscript dot represents the partial derivative with respect to time. L is the thickness of a plate and $u = z/L$ is the normalized depth.

We define the hydrodynamic relaxation time τ as

$$\tau=\lambda\left(\frac{\beta\eta L^2}{kK_p}\right) \tag{7}$$

with

$$\lambda=\frac{(1-b)(b-\phi)}{\beta}+b^2 \tag{8}$$

and the reduced time θ as

$$\theta=\int_0^t\frac{dt}{\tau} \tag{9}$$

As explained in the Supplementary material, from the solution of Eq. (6), we can obtain an implicit solution for the average pressure

$$\langle P[u,\theta]\rangle-P_A[\theta]=-\frac{\phi K_p}{b-\phi+b\phi}\int_0^\theta\beta_T[\theta']\frac{\partial\langle P\rangle}{\partial\theta'}\Phi[\theta-\theta']d\theta' \tag{10}$$

The average volumetric strain is given as

$$\langle\varepsilon\rangle=\frac{b\langle P\rangle-P_A}{K_p} \tag{11}$$

Combining Eq. (10) with Eq. (11) and considering the fact of $K_s \gg K_F$, the average strain can be simplified as

$$\langle\varepsilon\rangle\approx-\frac{b\phi}{b-\phi+b\phi}\int_0^\theta\beta_T[\theta']\frac{\partial\langle P\rangle}{\partial\theta'}\Phi[\theta-\theta']d\theta' \tag{12}$$

A good approximation for long times is given as

$$\Phi[\theta] = e^{\theta(3.26u-3.12)} \tag{13}$$

The final goal of depressurization is to keep the average volumetric strain below the maximum tolerable strain of the material:

$$\langle \varepsilon \rangle < \varepsilon^{max} \tag{14}$$

To avoid microcracking in Portland cement paste, the maximum tensile strain should be in the range of 60 - 200 $\times 10^{-6}$ [45]. We let $\varepsilon^{max} = 10^{-5}$ which should be a very conservative choice. Cement pastes with w/c = 0.4 - 0.5 have liquid permeability in the order of magnitude of 10^{-21} m^2 [46, 47, 48, 49, 50, 51], and gas permeability is considered around 10^{-17} m^2 [52, 53]. A supercritical fluid has a density close to that of a liquid, but transport properties close to a gas so letting $K = 10^{-20}$ m^2 will provide a conservative estimate of the acceptable depressurization rate. Considering depressurization starting at 8 MPa and 40 °C, we predict that the depressurization kinetics shown in Figure 8 will satisfy Eq. (14) for a 1-mm thick plate of paste.

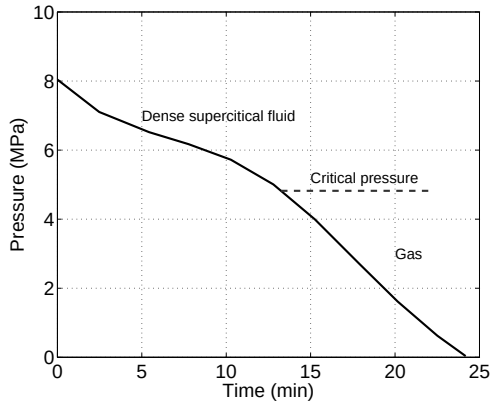

Figure 8: Calculated depressurization curve for 0.5 mm thick cement paste (drying from one side).

Three stages are clearly shown in Fig. 8. In the first stage, R23 is a dense fluid whose density does not change too much with pressure, so the pressure can drop relatively quickly without risking expansion of the paste. In the second stage, close to the critical pressure, fluid properties change sharply. The pressure drop must be much slower to provide a smooth transition from supercritical fluid to the gaseous phase. Below the critical point, R23 is in the gaseous phase and pressure decreases faster but not as fast as the first stage. The main reason is that the gas volume expands significantly with the decrease of pressure, but the bulk modulus of the fluid is low, so the stress imposed on the solid network is acceptable.

6. Experiment procedure

6.1. Sample preparation

In the present study, we only focus on samples at very early age (< 24 hrs). To observe the microstructure of hydration products by SEM, crushed samples are commonly extracted from a large piece of material in the literature (e.g. [54]). Actually, the microstructure of these samples has been altered during the sample preparation. In this study, we cast the specimen directly onto the SEM stub to facilitate the transfer of the specimen to the SEM with minimal exposure of the supercritically dried sample to the atmosphere (see Fig. 9a for cement paste on a SEM stub). The conventional aluminum stub can react with the alkaline solution in cement pastes and release hydrogen gas, so we prepared stainless steel stubs. A 0.5-mm deep cup was cut into the stub which can prevent overflow of the liquid cement paste. When the fresh paste was put in the cup, a convex surface was created. The maximum thickness (in the central part) is less than 1 mm.

(a) Cement paste on a SEM stub

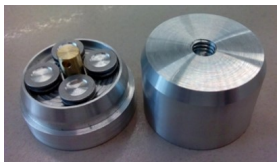

(b) Sample holder

Figure 9: Cement paste sample.

Curing condition has a significant influence on the development of the microstructure. Two main curing conditions were considered in this study: high RH and immersion in pore solution. The high RH condition was created by letting N_2 gas flow through the deionized water in a sealed humidity chamber. The actual RH measured by a UEi® digital psychrometer is above 99%. For this level of RH, small temperature variations can cause condensation of water on the surface of the specimen. To control temperature and minimize condensation, the humidity chamber was stored in an incubator at 25 °C. The pore solution is made from a recipe using 0.1062 M KOH, 0.0489 M Na_2SO_4, 0.037 M K_2SO_4, and 0.0212 M $Ca(OH)_2$ as a reasonable approximation of the ions in the cement paste [55, 56, 57]. After casting, the specimens were immediately transferred into a small container filled with the pore solution inside the incubator.

After curing for the desired length of time (1, 5, 10, 15, and 24 h), the specimens were taken out and submerged in isopropanol to replace water in the porous body. Isopropanol was renewed once in the first hour, once at ten hours and then the exchange continued until the drying tests. According to the calculation in Fig. 5, if the age of the specimen is less than one day and the thickness is less than 1 mm, the exchange can be completed in 4.2 hours. Therefore, an overnight exchange is more than sufficient.

6.2. Experiment recipe

During supercritical drying, two main factors must be well controlled: temperature and pressure. Based on the above discussion, we create the recipe shown in Fig. 10 for drying of 1-mm thick cement paste. There are four stages for the control of pressure:

(1) The initial pressurization. This step is to prepare the exchange condition. Pressure is increased from atmospheric pressure to about 5 MPa so that the gaseous R23 becomes liquid. The pressurization generally risks the least damage to the porous body; therefore, this step can be done in a short time (30 min in our recipe).

(2) Isopropanol/R23 exchange. Temperature and pressure are controlled in a stable condition (5 MPa and 25 °C) as R23 flows through the chamber. The concentration of isopropanol in the extractor gradually is decreased by the control valves until pure liquid R23 replaces all isopropanol. As calculated in Section 4, the isopropanol/R23 exchange is several times faster than the water/isopropanol exchange; thus, the exchange can be completed in one hour. Two hours are provided in the recipe to ensure complete replacement.

(3) Pressurization to supercritical fluid. As explained in Section 5.1, pressure is increased simultaneously with temperature to maintain constant liquid density during pressurization. Although quick pressurization generally has no effect on the solid body [41], this step should be done gently because it may take time to reach thermal equilibrium in the specimen. In this recipe, the highest pressure is set as 8 MPa (corresponding temperature 40 °C), much higher than the critical pressure of R23 (4.82 MPa), to avoid the sharp changes of fluid properties (density, viscosity, etc) when the condition is close to the critical point. Higher pressure and temperature can provide a stable fluid environment for further fluid evacuation.

(4) Depressurization. The depressurization curve in Section 5.2 shows that it takes about 25 min to evacuate supercritical R23 from a 1-mm thick sample, but we extend the pressurization duration to about 100 min. This greatly reduces the risk of damaging the solid body by diminishing the depressurization rate to about 1/4 of the calculated one. Temperature is maintained at 40 °C, which keeps the state of R23 always far from the critical point during depressurization (see Fig. 1).

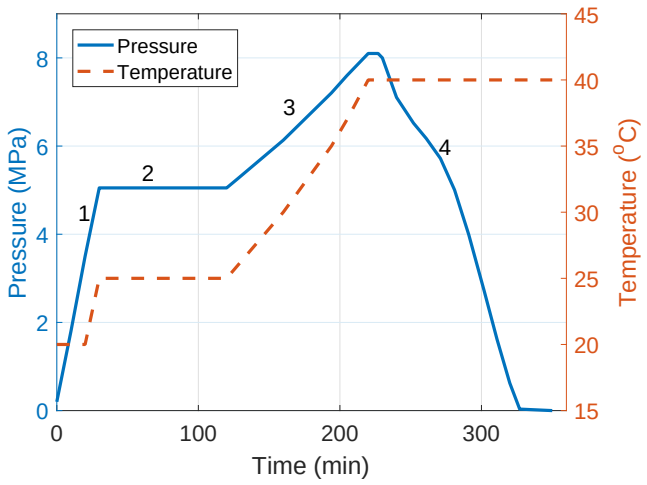

Figure 10: An example of experimental recipe for drying of 1-mm thick samples.

If the sample size is thicker than 1 mm or the sample is more mature (and consequently has lower permeability), one needs to use the isopropanol and R23 exchange data in Sections 3 and 5.2 to recalculate the experimental recipe.

6.3. Cycle control

The R23 exchange is carried out in a custom-designed computer-controlled autoclave shown in Fig. 11 which can precisely control pressure and temperature according to the recipe. In a test, the SEM stubs are secured on a stub holder (see Fig. 9b), which is heavy enough to stabilize the stubs. The stub holder is seated in the extractor (3). Prior to the test, the extractor is filled with about 200 mL isopropanol which is enough to ensure all samples being submerged. After the extractor is closed, the control computer (8) can automatically follow the recipe to change pressure and temperature.

The pressure control system is illustrated in Fig. 12. To drive the whole system, the supply pump (9) always provides 10.5 MPa to the inlet control valve (5) of the extractor. According to the recipe, the inlet valve can open to increase pressure in the extractor during pressurization and flush the extractor during isopropanol/R23 exchange. When pressure in the extractor is higher than the recipe, the outlet valve (6) will open to release pressure. The fluid flows into the separator (4), where alcohol condenses and R23 is distilled into the storage vessel (2). Most of the time during a run, pressure in the separator is the same as the pressure in the storage vessel. Due to the low temperature in the storage vessel and relatively high temperature in the separator, R23 vaporizes in the separator and condenses into the storage vessel; isopropanol remains in the separator because of its low vapor pressure. During the depressurization, when pressure in the extractor decreases to a point close to the pressure in the separator, the recycle pump is needed to push fluids from the separator to the storage vessel so that the pressure in the separator is always lower than that in the extractor. After a run, liquid R23 is kept in the storage vessel. Temperature control is easier than that for pressure. Two valves, one for cold water and one for hot water, are operated by the computer program to mix cold and hot water to provide the temperature specified in the recipe.

After the drying cycle, an extension rod with threads is used to carry the stub holder cap into the extractor and cover the holder to avoid air contact. Samples are then directly moved to the SEM or stored in a N_2 filled drying chamber until the SEM imaging.

6.4. R23 distillation

Liquid R23 is reused for each test so it may be contaminated by isopropanol. Low purity of R23 would reduce the efficiency of isopropanol/R23 exchange and leave isopropanol in the microstructure. In the initial test, we only collected about 90% isopropanol from the separator, meaning that about 10% isopropanol was mixed with R23 or still in the vapor phase in the autoclave. One main loss happens when the recycle pump is running. This pump creates a very low pressure environment (close to atmospheric pressure) that can enhance the vaporization of isopropanol

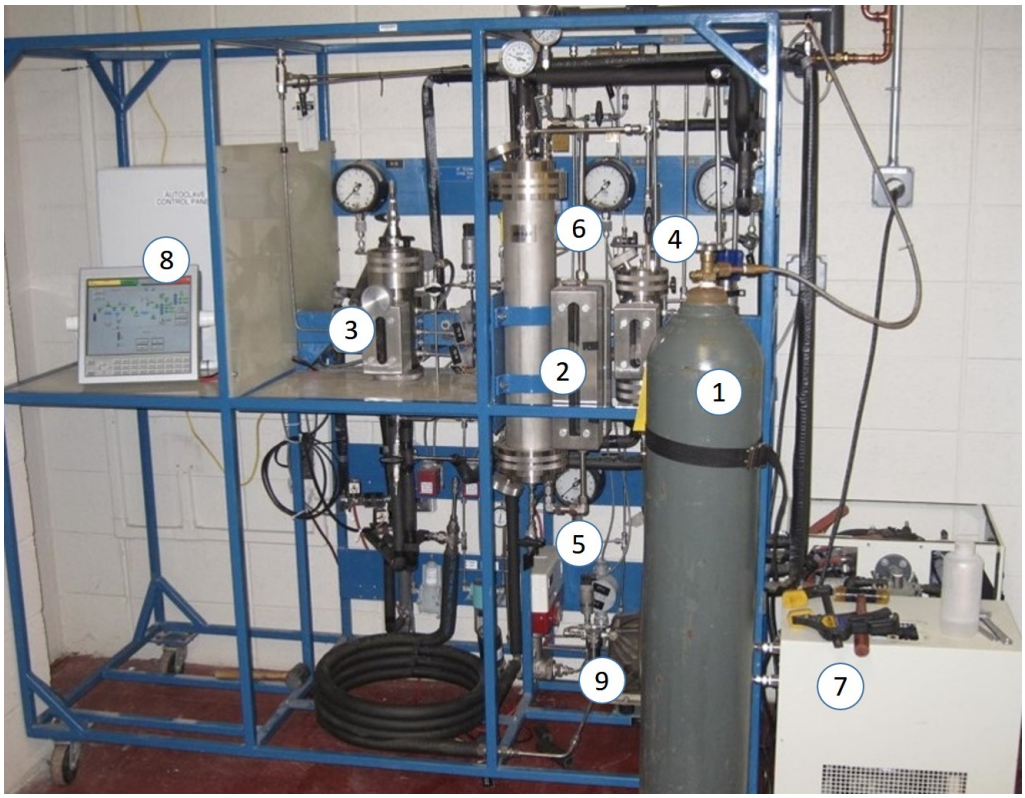

Figure 11: Autoclave. The main components are: 1 - Gas supply cylinder; 2 - Storage vessel (temperately storing liquid R23); 3 - Extractor (where the sample is in); 4 - Separator (separating isopropanol and R23); 5 - Extractor inlet control valve; 6 - Extractor outlet control valve (hidden by the storage vessel); 7 - Cooling/heating system; 8 - Control computer; 9 - Supply pump (partially hidden by the gas supply cylinder). The recycle pump is not shown in this photo.

which then condenses in the storage vessel. The solution is to collect isopropanol from the separator before running the recycle pump. The only drawback is that some R23 will run out from the separator because it is still pressurized. After this step, the loss of isopropanol can be reduced to about 5%.

To further purify liquid R23, a distillation process is needed by only allowing R23 to circulate between the separator and the storage vessel. No fluid goes into the extractor (fluid follows the black dashed line in Fig. 12). When the highly pressurized fluid enters the separator, the endothermic process can lead to condensation of both isopropanol and R23 while the heating from the bottom of the vessel is able to vaporize R23. By using a needle valve to control the flow rate to the separator, the condensation of isopropanol can be maximized. After the distillation, the loss of isopropanol is reduced to about 1%.

7. Results

7.1. SEM images

SEM imaging is a very useful way to provide visual information about the microstructure of hydration products in cement pastes. In this study, we used the FEI Quanta 200 ESEM, which has high resolution to see the details of the microstructure of the hydration phases. After drying, a 10 nm thick iridium coating is applied to the surface of the specimen to increase the conductivity. In ESEM, the low vacuum mode is used to reduce the charging problem and also prevent the damage due to high level of vacuum. For comparison purposes, two conventional drying methods, flowing N_2 drying and isopropanol replacement followed by flowing N_2 (hereafter called IPA drying), were also carried out for some samples.

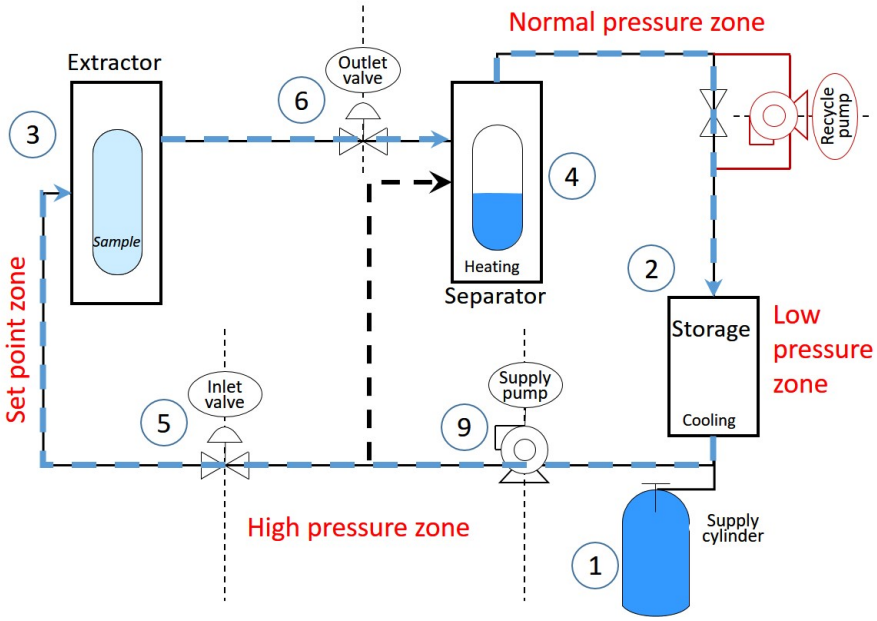

Figure 12: Control system (mainly showing the pressure control system) and flow direction during the exchange (dashed lines). Thermal transducers, pressure gauges and other small valves are not shown in this figure. The numbering is the same to Fig. 11.

SEM images of the external surface of samples cured in the high RH chamber are shown in Fig. 13. Note that the present paper only focuses on the morphology of the exterior surface, and SEM images for the interior will be reported in our following paper [58]. It is clear that the needle-/fiber-like C-S-H grows on the surface of cement particles from very early age (e.g. 1 h). A similar structure has been reported by other researchers (e.g. [59, 60, 61]), except that fibers are much longer in our images. This structure is well preserved in SCD, while it seems to be damaged by IPA drying. This might be due to the fact that hydration products are extremely weak at this age so the presence of capillary pressure can easily cause needles to collapse onto the cement grain. At 5 h, the shape of the fibers is quite similar to that at 1 h, but it is much denser in terms of the number of fibers in a unit area. Compared to SCD and IPA methods, flowing N_2 drying is the worst method in which the fibrous structure totally collapses and creates large pores and denser solids because of the capillary forces.

After hydration for 10 h, fibers are much thicker and stronger, like several thin fibers twisted together. In fact, the observed morphology is quite similar to the interleaved and interlocked foil structure reported by Jennings et al [59]. SCD still shows an advantage in terms of preserving the fibrous structure. This structure in IPA dried samples collapses, but we still can see the short fibers radiating perpendicularly from the cement grains. The comparison indicates that, even though IPA has lower surface tension than water, the capillary force is still high enough to damage the microstructure of hydration products. At 15 h, the surface becomes very uniform and seems to be covered by a thin solid film. It looks like the gaps between fibers are filled with some solids. Energy Dispersive X-Ray Analysis (EDX) shows that main elements from the surface are O and Ca as well as a small amount of Si, which means the solid cover is a mixture of C-S-H and calcium hydroxide.

Compared with SEM images in the literature [59, 60, 61], our images show two main differences: a) Fibers/needles develop much earlier and are longer; b) The surface finally becomes very smooth. The formation of these kinds of structures can be explained by the theory of "whisker growth" (e.g. [62]). Even though the RH in the chamber is as high as 99%, water from the sample surface still continuously evaporates during curing. The evaporation causes the accumulation of ions in the surface solution which favors the growth of C-S-H. That is why we see long C-S-H fibers at 1 h. With the growth of hydration products, the gaps between fibers become smaller and smaller, and then they are filled with liquids (pore solution) due to the capillarity. In a manner similar to "whisker growth", liquids deposit solids during evaporation. At 5 and 10 h, this kind of structure has already started growing from the parts close to the cement grains (see the central solid parts) and it continues to develop until the whole surface is covered by the solid

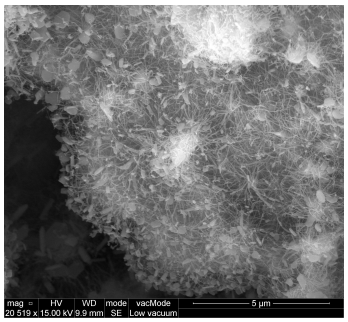

(a) SCD, 1 h

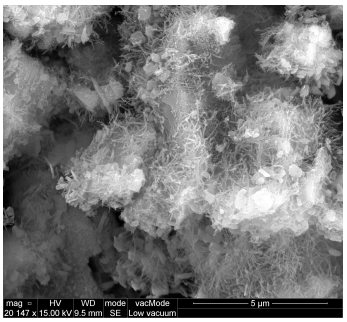

(b) IPA, 1 h

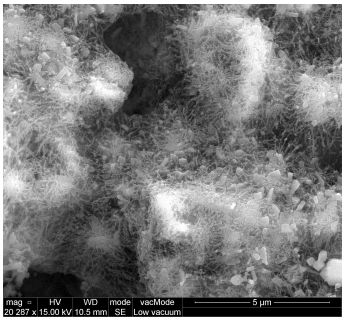

(c) SCD, 5 h

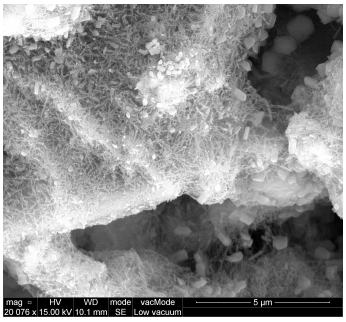

(d) IPA, 5 h

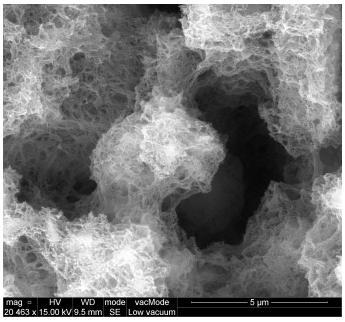

(e) Flowing N_2, 5 h

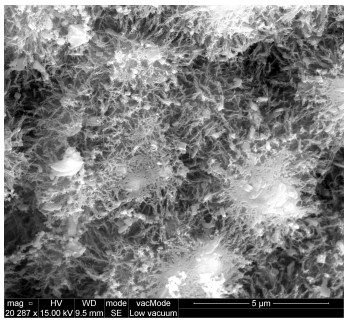

(f) SCD, 10 h

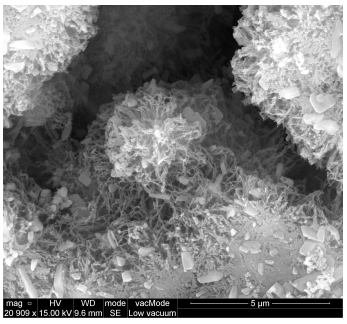

(g) IPA, 10 h

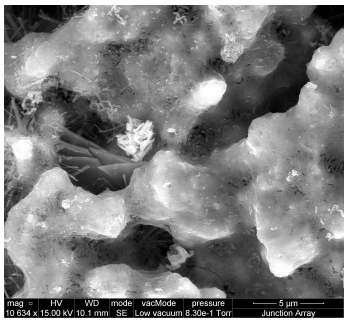

(h) SCD, 15 h

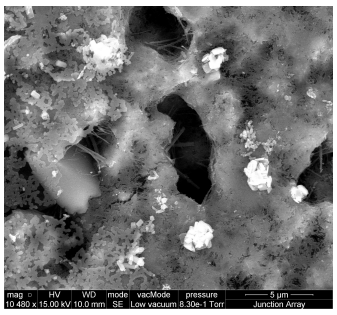

(i) IPA, 15 h

Figure 13: SEM images for the external surface of cement pastes, cured in the high RH chamber, w/c = 0.5 at different ages. Note that the magnification for 15 hours is lower than that for other ages. For the high quality SEM images, we refer readers to the web version of this paper.

film. At this age, the only difference between the drying methods is the drying cracks formed on the surface of IPA dried sample (see Fig. 13i). There is also a large amount of calcium hydroxide crystallized on the surface due to the water evaporation.

Figure 14 shows SEM images of the external surfaces of samples cured while submerged in pore solution. The structure is obviously different from samples cured in the high RH chamber. At 1 h, some C-S-H flakes, hexagonal calcium hydroxide crystals and a few ettringite needles can be seen on the surface. Compared to samples cured in the humid chamber, hydration products are few and we could not see differences between the selected drying methods. This supports the idea that the growth of the long C-S-H fibers in Figs. 13a and b is expedited by evaporation at the surface. At the later ages, flakes of C-S-H gradually grow from the surface and combine to form the sheet-like structure that totally covers the surface of the clinker particle. The sheets look like the "honeycomb" structure reported by Menetrier et al. for C3S hydrated in water for 3 hours [63], especially for the flowing N_2 dried sample. We believe that the small pores in the "honeycomb" are created by capillary forces from the harsh drying method, because SCD and IPA dried samples do not show so many pores. Additionally, cracks are observed on the surface for IPA and flowing N_2 dried samples. At 24 hours, the C-S-H structure is different from the previous ages, but it is still very clear that flowing N_2 dried samples shows a more compacted structure than the other drying methods.

The synthetic pore solution provides a chemical environment similar to that inside the cement paste; thus, the C-S-H microstructure is expected to be the same as that reported in the literature [59, 60, 61]. To the best of our knowledge, this sheet-like microstructure is rarely reported in the literature. A possible reason is that the Ca/Si ratio on the surface is lower than that in the cement paste, as Kalousek and Prebus reported that no fibrils appeared if the Ca/Si ratio < 1.5 [64].

7.2. BET surface area

SEM images cannot provide quantitative information about the microstructure, so we use the BET surface area to compare the effects of the drying methods. The general expectation is that the higher BET surface area, the better microstructure is preserved. In the other words, a smaller BET surface area tells us that the microstructure is altered. This hypothesis is questioned by some researchers [3], but so far no experimental evidence is able to prove that a drying method can lead to a more complex microstructure that would provide higher BET surface area.

The sample preparation for nitrogen adsorption is different from that for SEM imaging, because a large amount of sample is required. To get enough materials, the cement pastes were cast in a cylinder with diameter 8 mm. After a certain period of sealed curing, the cylindrical pastes were demoulded, crushed and sieved. The size of the particles used for nitrogen adsorption is between 0.6 and 1.2 mm. Because the specimens are young, they can be easily dried during preparation; thus, specimens for SCD and IPA drying were crushed and sieved in isopropanol. Before transfer to the autoclave for SCD, the granular materials were rinsed several times by isopropanol to remove any fine particles that must be prevented from entering the control valves in the autoclave.

After drying, samples should be subjected to nitrogen adsorption as soon as possible (less than one day) to minimize the storage influence as Rarick et al. [65] have pointed out that storage time might decrease the measured BET surface area. Nitrogen adsorption measurements were conducted by using an ASAP 2020 apparatus, from Micromeritics®. Calibration with aluminum oxide showed that when the sample has a surface area of 5 - 10 m^2 the apparatus provides reliable results so the weight of sample 0.5 g was used for all tests in this study. Prior to adsorption, a degassing process was needed to clear any impurities, normally physisorbed molecules, such as O_2, CO_2 and the residual evaporable water that was not removed by drying. It has been found that different levels of degassing could affect the measured results because the degassing is actually a vacuum drying process [15]. If the samples are not fully dried before degassing, capillary pressure still exists and is harmful to the microstructure. For the purpose of comparison, the same degassing level at 5 μmHg was used for all tests. BET surface area is calculated based on the adsorption curve between 0.05 and 0.3 relative pressure.

An important implication from Fig. 15 is that samples dried by flowing N_2 always provide the lowest surface area. This is in agreement with the conclusion drawn by most studies that the direct drying method can cause significant damage to the microstructure. Actually, Figs. 13 and 14 clearly show the compacted microstructure induced by capillary pressure for the flowing N_2 dried samples, regardless of the curing conditions. Although SEM images show that the microstructure may be altered by isopropanol replacement, the BET area difference between SCD and IPA drying is relatively small. Only at 24 h, isopropanol replacement shows a slightly higher surface area than SCD. Hence, we do not see a significant difference between SCD and IPA drying for samples younger than one day of hydration.

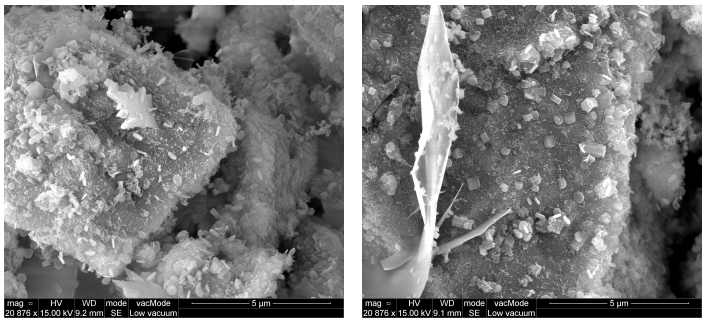

(a) SCD, 1 h (b) IPA, 1 h

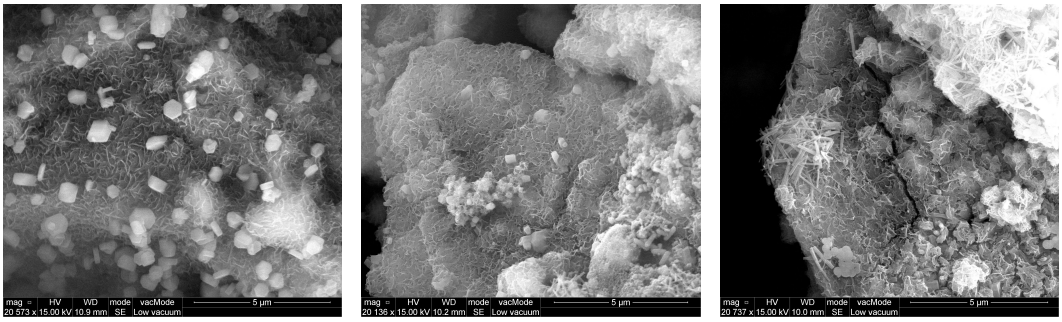

(c) SCD, 5 h (d) IPA, 5 h (e) Flowing N_2, 5 h

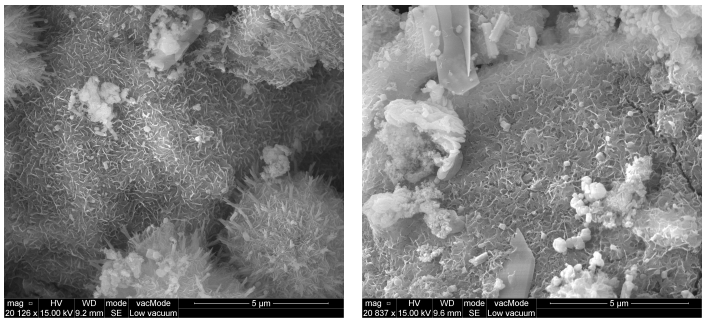

(f) SCD, 10 h (g) IPA, 10 h

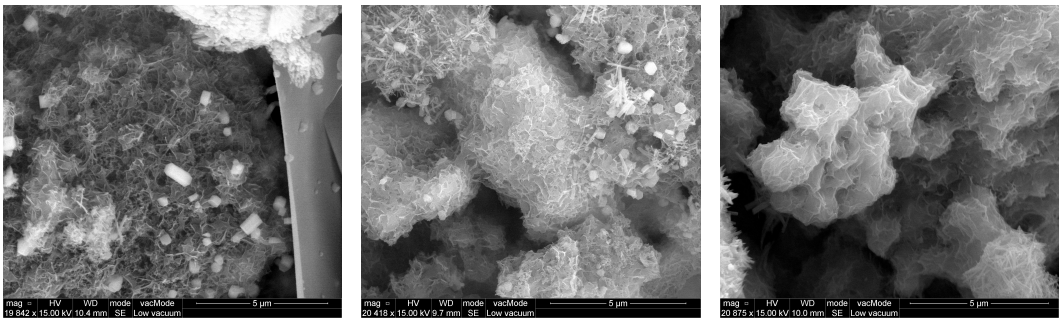

(h) SCD, 24 h (i) IPA, 24 h (j) Flowing N_2, 24 h

Figure 14: SEM images for the external surface of cement pastes w/c = 0.5 at different ages, cured in the pore solution.

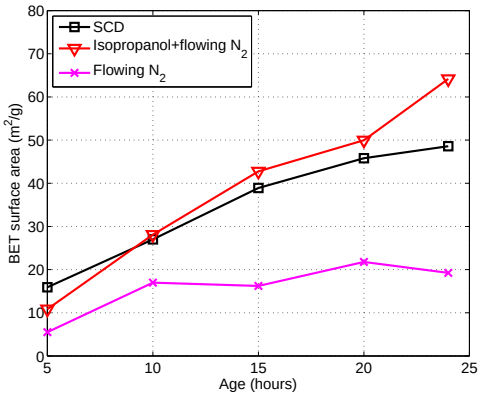

Figure 15: BET surface area measured by nitrogen adsorption.

8. Discussion

SCD has been successfully applied for drying of cementitious materials. Nevertheless, some questions still remain open for discussion, such as shrinkage during isopropanol replacement, and the chemical impact of isopropanol and R23 on the chemical compositions of the cement pastes.

8.1. Isopropanol diffusion induced shrinkage

The shrinkage of cement paste exchanged with isopropanol has been reported in the literature (e.g. [66]), but we do not know whether the microstructure has been damaged during the dimensional change. In this study, the length change of cylindrical specimens was measured by a dynamic mechanical analyzer (DMA): a sample containing pore water is mounted in the DMA and a cup containing IPA is gently raised to submerge the sample. The initial length of the specimen is about 2.2 cm. Two diameters have been tested, 6 mm and 8 mm. The age effect was also considered.

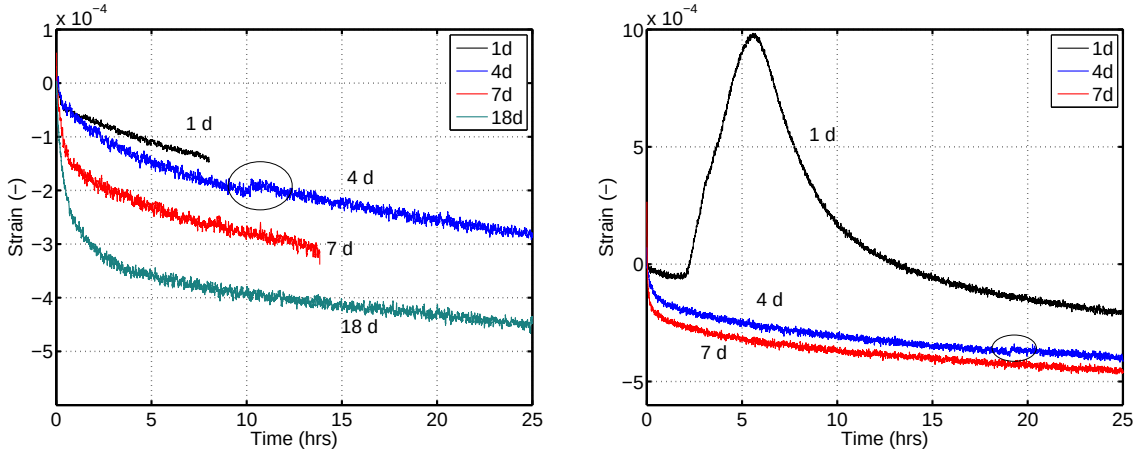

(a) Specimens 6-mm diameter

(b) Specimens 8-mm diameter

Figure 16: Measured strain curves for specimens immersed in isopropanol at different ages. Ellipses indicate the small jumps. The jump is much obvious for the 1-d old 8-mm specimen.

Figure 16 compares measured strain curves for different sizes of specimens at different ages. All tested specimens contract regardless of ages and diameters. The shrinkage may be explained by the following mechanisms:

(1). Chemical reaction. Isopropanol reacts with cement pastes. This is widely accepted by researchers although no reaction product has been identified.

(2). Different diffusion coefficients of water and isopropanol. If water diffuses out more rapidly than isopropanol diffuses into the paste, the material will contract due to the resulting suction in the porous body. If this is the real case, the material will recover when isopropanol gradually enters the interior of the material. However, our tests do not show the expansion even though the specimen was immersed in isopropanol more than a week.

(3). Osmotic extraction. Since the molecule of isopropanol is larger than water, water can diffuse out of the C-S-H inter-layer sheets, but isopropanol can not move into these sheets. As a result, the shrinkage occurs. This theory has been used to explain the expansion of cement pastes immersed in methanol, because the size of the methanol molecule is smaller so it can enter the small gaps between C-S-H sheets to cause the expanision [67].

After isopropanol exchange, the specimen was immersed in water for a second exchange to replace isopropanol. As shown in Fig. 17, the specimen starts expanding when it is put in water. But the final strain is still negative (zero is the original strain), meaning that the material is still contracted. The implication is that the dimensional change caused by IPA exchange is partially irreversible. This could be a purely physical effect, analogous to the contraction that occurs during the first drying of a paste, which results in some plastic deformation. On the other hand, some organic material is retained following IPA drying [3], so we cannot exclude the possibility that the contraction is at least partially caused by a chemical reaction. We also note that the rate of expansion (in water) is much higher than the shrinkage (in isopropanol). This indicates that the diffusion of water is faster than isopropanol. Hence, we might conclude that the first and second mechanisms mentioned above may coexist to cause the contraction during isopropanol exchange.

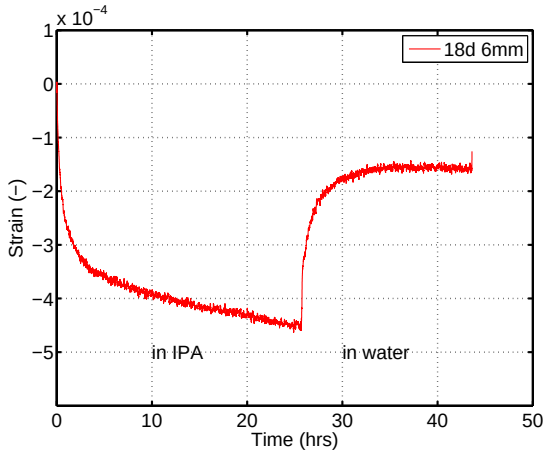

Figure 17: Measured strain curves for specimens immersed in IPA and then in water.

In Fig. 16, it can be seen that some curves jump during the exchange with isopropanol. We suspect these jumps are related to the slow development of microcracks. It seems that the damage to 8-mm specimen is larger than that to 6-mm specimen (see the large jump for the 1-d old 8-mm specimen), which would be associated with a larger concentration (and strain) gradient in the thicker cylinder. Furthermore, cracking tends to occur for specimens at young age, such as at 1 and 4 days. At these ages, the specimen starts becoming rigid but has not yet developed enough strength to resist the pressure created by isopropanol exchange. This may imply that the use of small specimens can reduce the risk of damaging to the solid body. In this study, we used 1-mm samples for SCD, which should be on the safe side. Besides, the adhesion between the paste and stub is very weak so that the radial stresses are avoided by slippage of the paste on the substrate.

8.2. Chemical impact of isopropanol

The chemical impact of isopropanol on cement pastes reported in the literature are mostly based on the observation of dimensional changes. Hughes [67] and Hughes and Crossley [68] found that the immersion of specimens in

isopropanol yields unexpected non-monotonic weight changes. They concluded that this could be due to chemical interactions of isopropanol with the cement paste during penetration of isopropanol into the cement matrix. Length changes reported by Beaudoin et al. [69] were used to indicate that isopropanol can react with calcium hydroxide. However, their tests also show that isopropanol has the least effect on the dimensional change, compared to methanol, acetone and benzene. Hence, among common solvents, isopropanol is still the best one to use. Based on the assumption that isopropanol can react with cement, we attempt to identify the reaction products by using techniques, such as thermogravimetric analysis (TGA), Fourier transform infrared spectroscopy (FTIR) and X-ray diffraction (XRD).

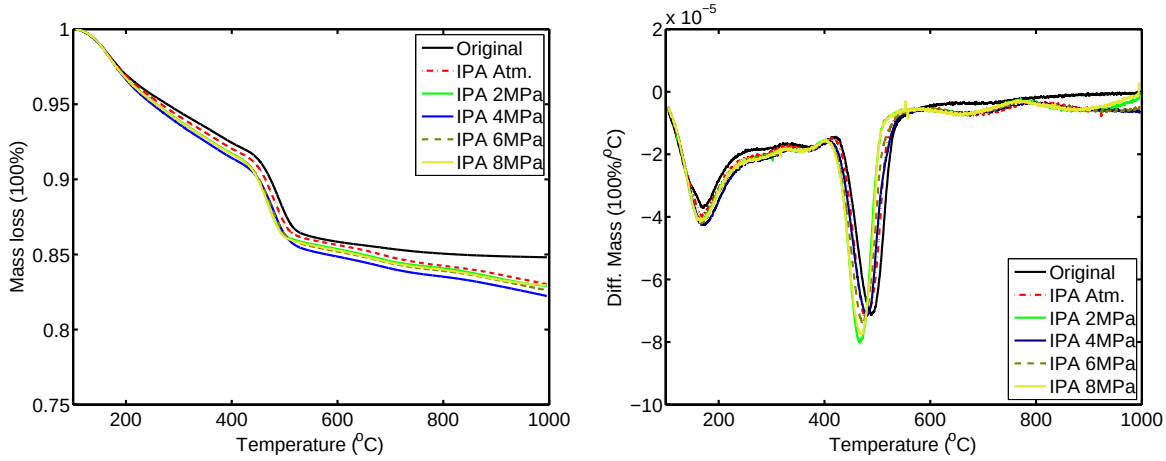

(a) TGA mass loss curves.

(b) Derivative mass loss.

Figure 18: TGA curves for 14 d samples immersed in IPA for 4 hours at different pressures.

During SCD, samples endure high pressure in the vessel with isopropanol. Here, a series of tests were carried out to check whether the pressure can enhance the chemical impact. Samples were submerged in isopropanol in the extractor (see Fig. 11). A N_2 cylinder with a pressure regulator was used to provide a specified pressure. Test duration is 4 hours and temperature is set at 40 °C, the same as in the SCD procedure. Prior to the tests, the 14-d old samples were subjected to isopropanol exchange for two days at atmospheric pressure and room temperature. After pressurizing in the autoclave, samples were dried by the flowing N_2 for one day and then heated in the TGA (PerkinElmer® Pyris 1) with the following temperature process: (1) heated to 105 °C at 10 °C/min from room temperature; (2) held for 30 min; (3) heated to 1000 °C at 5 °C/min [3]. The second step is supposed to remove all evaporable water. The measured TGA mass loss and the corresponding derivative curves are shown in Fig. 18. It is clear that the mass loss for the original (unexchanged) sample is always smaller than that of isopropanol-treated samples. The larger mass loss may be due to the strong interaction between isopropanol and cement paste. After the calcium hydroxide decomposition peak (480 - 500 °C), the curve for the original sample quickly reaches a plateau. In contrast, curves for isopropanol-treated samples are still decreasing, and the derivatives of these curves show two peaks at 670 and 900 °C, which correspond to the thermal decomposition of carbonate-like materials.

To further analyze the chemical impact of isopropanol, FTIR (PerkinElmer® Frontier) was used to identify the gas emitted from TGA. FTIR spectra for the samples heated at different temperatures are shown in Fig. 19. We can see two main isopropanol peaks at 77 and 105 °C, and there is still a trace of isopropanol released from the material at 158 °C. This means that isopropanol needs higher temperature to be removed than water. This supports the argument that IPA interacts with cement more strongly than water so that the complete removal of isopropanol is difficult to achieve. At higher temperatures, only peaks for CO_2 and H_2O can be seen in FTIR spectra, and the CO_2 peak seems to be gradually increasing. Correspondingly, the TGA mass loss curve is decreasing in Fig. 18a.

The chemical impact of isopropanol may happen in several ways: 1) Isopropanol directly reacts with cement paste (most likely with calcium hydroxide); 2) The decomposition products of isopropanol can react with cement paste at high temperature during the heating of samples in the TGA; 3) Other more complicated chemical/physical processes may be involved. By using various techniques (XRD, FTIR, TEM, etc), Rodriguez-Navarro et al. [71]

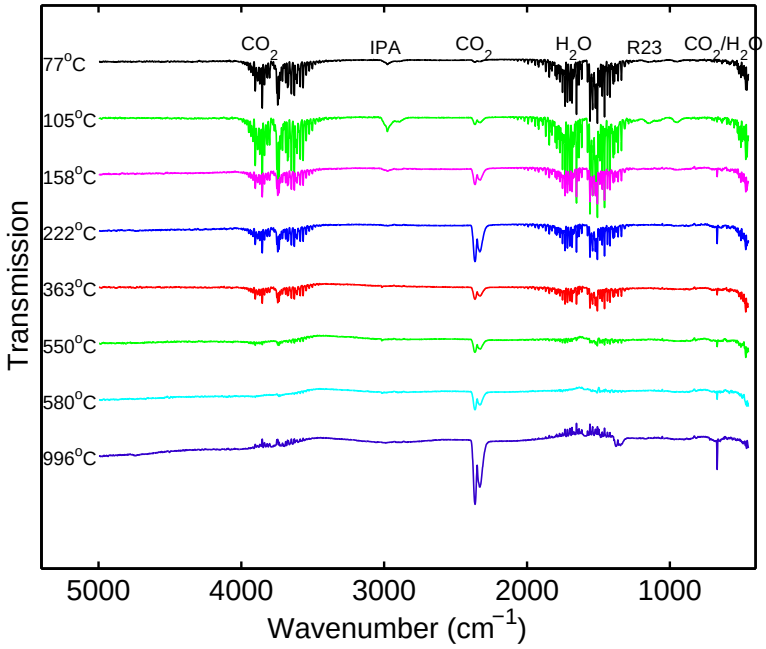

Figure 19: FTIR spectra for emitted gas when the IPA dried sample is heated by TGA. The sample age is 14 days and exchanged with isopropanol at atmospheric pressure. Peaks are identified by the spectrum analysis software provided by PerkinElmer® and the online database from NIST [70].

concluded that the assumption of isopropanol reacting with calcium hydroxide resulting in the formation of calcium isopropoxide ($Ca(OCH(CH_3)_2)_2$) is most reasonable. This kind of reaction is reversible depending on temperature and the presence of water; that is, when water is gradually removed by isopropanol exchange or heating in TGA, more calcium isopropoxide is formed in the material:

$$Ca(OH)_2 + 2CH_3CHOHCH_3 \leftrightarrows Ca(OCH(CH_3)_2)_2 + 2H_2O \tag{15}$$

However, XRD patterns of the isopropanol-treated cement paste do not show any extra peaks that could correspond to the crystalline calcium isopropoxide in Fig. 20. It may be because the newly formed isopropoxide is poorly crystalline or too low in quantity to be detectable by XRD.

Using data in Fig. 18 to calculate the mass loss due to the decomposition of calcium hydroxide (temperature between 400 and 550 °C), we have the results: 5.65% (Original), 5.48% (Atm.), 5.85% (2 MPa), 5.80% (4 MPa), 5.66% (6 MPa) and 5.37.% (8 MPa). These values are very close; thus, the chemical impact of isopropanol on calcium hydroxide is less significant than what was reported by Rodriguez-Navarro et al. [71]. Additionally, Fig. 20 shows identical XRD patterns for IPA dried and flowing N_2 dried samples, meaning that the chemical impact on other components of cement paste can be neglected.

Is it possible that interaction of isopropanol with cement paste is enhanced by the heating in TGA? Trenwith [72] reported that at temperatures in the range 448 – 528 °C, the decomposition of isopropanol leads to "the formation of hydrogen and acetone, together with smaller amounts of water and propene". In theory, acetone can react with calcium hydroxide to form calcium acetate, but it is thermally decomposed at relatively low temperature (around 380 °C [73]). Consequently, calcium acetate can not be formed in the TGA. Moreover, the FTIR spectra do not show any peaks associated with acetone.

We believe that the influence of isopropanol on cement paste is a more complicated chemical/physical process. By using the techniques presented in this study, it is not possible to provide a clear explanation. Perhaps carbonation is accelerated by the presence of isopropanol or isopropanol is just strongly physical bonded with C-S-H and calcium hydroxide rather than reacted with them.

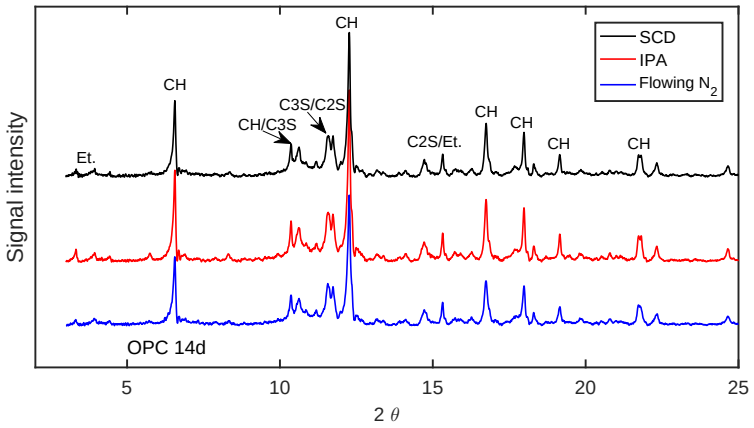

Figure 20: XRD curves for sample dried by different methods. The sample age is 14 days. The XRD instrument employs a Ag-tube to get high energy in the low 2θ range. Abbreviations are: Et. = Ettringite, CH = calcium hydroxide, C3S = tricalcium silicate and C2S = dicalcium silicate.

8.3. Chemical impact of R23

We used the same experimental methods as for isopropanol to investigate the chemical impact of R23 on the cement paste. The extractor, containing cement paste samples and isopropanol, was pressurized by R23 for about 4 hours at different pressure levels. Contrary to samples in pure isopropanol, TGA curves in Fig. 21 show that the total mass loss increases with the pressure applied to samples. Mass loss curves for 4 and 6 MPa are almost identical, which indicates that the chemical impact is independent of pressure above 4 MPa. The peaks related to the decomposition of carbonate-like products are more significant than in isopropanol-treated samples.

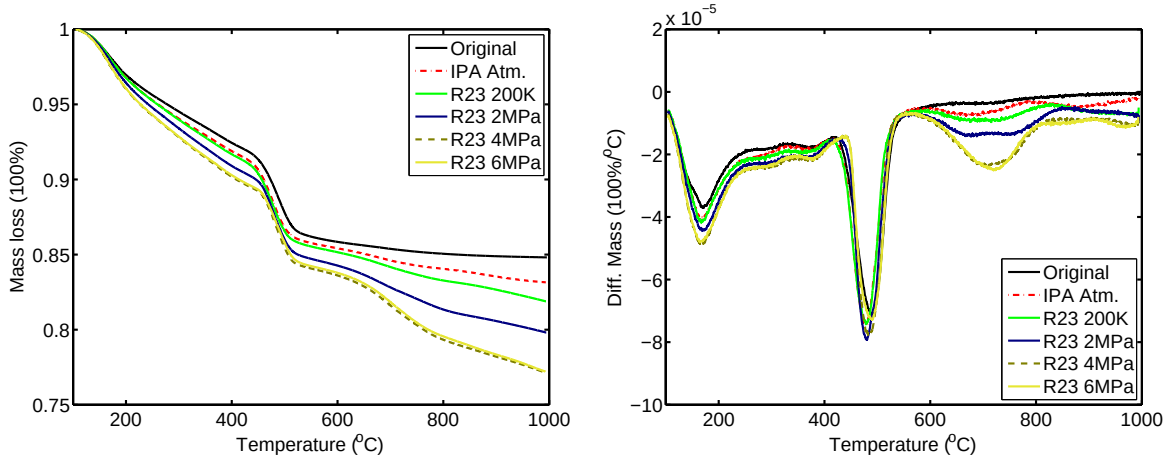

(a) TGA mass loss curves.

(b) Derivative mass loss.

Figure 21: TGA curves for 14d sample pressurized in R23 at different pressures. Prior TGA, the cement paste has been immersed in isopropanol for two days.

There is R23 remaining in the material after SCD as shown in the corresponding FTIR spectra (see Fig. 22). A small amount of R23 is released when samples are heated at 105 °C, and more can be seen when temperature increases to 265 °C which is much higher than the temperature required to remove isopropanol from cement paste. Accordingly, the interaction of R23 with cement paste is also stronger than that for isopropanol. Figure 22 also shows some isopropanol emitted at 105 °C, indicating that R23 exchange is not able to completely remove isopropanol.

A large CO_2 peak can be seen when samples are heated to 720 °C. The impact of isopropanol seems to be enhanced by the presence of R23. It can be explained by the fact that the molecular size of R23 (diameter 0.4 nm) is smaller

than isopropanol (diameter 0.5 nm) so that R23 can enter tiny pores (gel and interlayer pores) which isopropanol can not enter. With the higher external pressure, the openings of tiny pores are enlarged by the penetration of R23 and isopropanol may then be able to enter these pores. Hence, the influence of isopropanol also becomes more significant as revealed by the larger mass loss associated with the decomposition of carbonate-like products. Although SCD samples have been dried by the flowing N_2 and heating at 105 °C in the TGA, FTIR spectra show that isopropanol and R23 still exist in the tiny pores and can not be completely evacuated. This means that the tiny pores are blocked by the remaining isopropanol and R23, inhibiting access of N_2 molecules during nitrogen adsorption; therefore, the measured BET surface area is slightly lower than that for samples dried by isopropanol replacement. At very early ages (e.g. 5 and 10 h), the measured BET surface area for SCD samples is slightly higher than IPA dried samples, because at these ages a very small amount of tiny pores has developed and has less contribution to the total surface area.

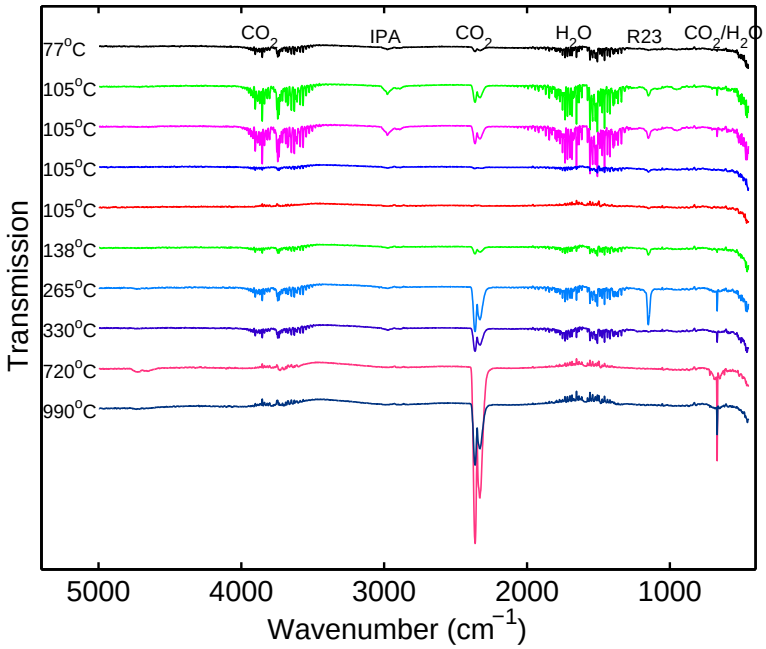

Figure 22: FTIR spectra for emitted gas when the SCD sample is heated by TGA. The sample age is 14 days.

Based on data in Fig. 21, the mass loss related to the decomposition of calcium hydroxide in the SCD samples is also calculated as 5.65% (Original), 5.48% (Atm.), 5.81% (200 KPa), 5.60% (2 MPa), 5.26% (4 MPa) and 5.31% (6 MPa). These values are more or less the same, which means that SCD does not have an obvious influence on calcium hydroxide. Similarly, the identical XRD patterns for SCD and flowing N_2 dried samples in Fig. 20 indicate the negligible impact of R23 on other components in the cement paste.

9. Conclusion

In this study, a new drying method - supercritical drying by using trifluoromethane (R23) - was developed. Main concerns, such as exchange duration, sample size, pressurization, depressurization, diffusion induced shrinkage and chemical impact, have been fully investigated, either by theoretical or experimental methods. Theoretically, SCD is an ideal drying method to preserve the microstructure of porous materials. This is confirmed by the SEM images which show less compact morphology for SCD than the other two conventional drying methods. Nevertheless, the BET surface area by nitrogen adsorption does not show significant difference between SCD and IPA drying. The main reason seems to be that isopropanol and R23 molecules enter the tiny pores (under pressure) and can not be removed by the flowing N_2 drying (zero RH) and vacuum applied prior to nitrogen adsorption, which causes these pores to be blocked and inaccessible to N_2 molecules.

Additional conclusions are as follows:

1. Based on the measured data and theoretical calculation, the diffusion coefficient of R23/isopropanol exchange is several times higher than water/isopropanol exchange. Therefore, the SCD loop needs relatively short duration.

2. After each test, a distillation process is needed to purify R23, which can largely decrease the isopropanol content in liquid R23.

3. The shrinkage induced by isopropanol is observed for young age and large diameter samples. The use of smaller specimens can reduce the risk of cracking. The shrinkage is probably caused by osmotic extraction of interlayer water by isopropanol. The kinetics of shrinkage indicate the faster diffusion rate for water than for isopropanol.

4. SEM images show significantly different morphology between specimens cured in high relative humidity chamber and in pore solution. The long and thin fibers observed on the surface of the specimens cured in the humidity chamber can be explained by the "whisker growth" theory. The sheet-like surface for samples immersed in pore solution may be related the different Ca/Si ratio between the pore solution and the interior of a specimen.

5. The chemical impact of isopropanol and R23 on cementitious materials was investigated by TGA, FTIR and XRD. The whole picture of chemical impact is still not clear, but one certain finding is that isopropanol and R23 have very limited influence on calcium hydroxide. XRD patterns also do not show any sign that isopropanol and R23 react with other components in the cement paste.

We must note that the supercritical drying proposed in this study uses trifluoromethane (R23) as the drying fluid. This is the most suitable candidate within the Freon® family, owing to its low critical temperature and pressure. There might be other compounds, of which we are unaware, that would have less interaction with cementitious materials. If so, the theories provided in this study are still valid and should be repeated to evaluate the possible modifications of the microstructure caused by chemical reactions during exchange and drying.

Acknowledgment

This work was supported by funding from Federal Highway Administration (FHWA) through the program DTFH61-12-H-00003 and NSF grant CMMI-1335320. The authors thank our collaborators at Oklahoma State University, National Institute of Standard and Technology, University of California in Santa Barbara, University of Bremen and W.R. Grace. The authors appreciate the effort of the senior technician Joseph Vocaturo to modify the autoclave. The authors also thank Prof. Claire White for allowing us to use the XRD instrument.

References

[1] H. M. Jennings, J. J. Thomas, J. S. Gevrenov, G. Constantinides, F.-J. Ulm, A multi-technique investigation of the nanoporosity of cement paste, Cement and Concrete Research 37 (2007) 329–336.

[2] K. Aligizaki, Pore Structure of Cement-Based Materials: Testing, Interpretation and Requirements, Taylor & Francis, London and New York, 2006.

[3] J. Zhang, G. W. Scherer, Comparison of methods for arresting hydration of cement, Cement and Concrete Research 41 (2011) 1024–1036.

[4] M. Suzuki, S. Maeda, On the mechanism of drying of granular beds - mass transfer from discontinuous source, J. Chem. Eng. Japan 1 (1968) 26–31.

[5] G. Scherer, Drying, shrinkage, and cracking of cementitious materials, Transp. Porous Med. 110 (2015) 311–331.

[6] S. Mantellato, M. Palacios, R. J. Flatt, Impact of sample preparation on the specific surface area of synthetic ettringite, Cement and Concrete Research 86 (2016) 20–28.

[7] L. Konecny, S. J. Naqvi, The effect of different drying techniques on the pore size distribution of blended cement mortars, Cement and Concrete Research 23 (1993) 1223–1228.

[8] X. Wang, A. Eberhardt, E. Gallucci, K. Scrivener, Assessment of early age properties of cementitious system through isopropanol–water replacement in the mixing water, Cement and Concrete Research 84 (2016) 76–84.

[9] R. Day, Reactions between methanol and portland cement paste, Cement and Concrete Research 11 (1981) 341–349.

[10] J.J.Beaudoin, Validity of using methanol for studying the microstructure of cement paste, Materials and Structures 20 (1987) 27–31.

[11] H. Taylor, A. Turner, Reactions of tricalcium silicate paste with organic liquids, Cement and Concrete Research 17 (1987) 613–623.

[12] G. Scherer, Freezing gels, Journal of Non-Crystalline Solids 155 (1993) 1–25.

[13] C. Galle, Effect of drying on cement-based materials pore structure as identified by mercury intrusion porosimetry: A comparative study between oven-, vacuum-, and freeze-drying, Cement and Concrete Research 31 (2002) 1467–1477.

[14] N. Collier, J. Sharp, N. Milestone, J. Hill, I. Godfrey, The influence of water removal techniques on the composition and microstructure of hardened cement pastes, Cement and Concrete Research 38 (2008) 737–744.

[15] A. Korpa, R. Trettin, The influence of different drying methods on cement paste microstructures as reflected by gas adsorption: Comparison between freeze-drying (f-drying), d-drying, p-drying and oven-drying methods, Cement and Concrete Research 36 (2006) 634–649.

[16] R. Feldman, Diffusion measurements in cement paste by water replacement using propan-2-ol, Cement and Concrete Research 17 (1987) 602–621.

[17] D. Snoeck, L. Velasco, A. Mignon, S. V. Vlierberghe, P. Dubruel, P. Lodewyckx, N. D. Belie, The influence of different drying techniques on the water sorption properties of cement-based materials, Cement and Concrete Research 64 (2014) 54–62.

[18] S. Kistler, Coherent expanded aerogels, J. Phys. Chem. 36 (1931) 52–64.

[19] M. A. Aegerter, N. Leventis, M. M. Koebel, Aerogels Handbook, Springer-Verlag, New York, 2011.

[20] G. G. Litvan, Variability of the nitrogen surface area of hydrated cement paste, Cement and Concrete Research 6 (1976) 139–144.

[21] L. J. Parrott, Thermogravimetric and sorption studies of methanol exchange in an alite paste, Cement and Concrete Research 13 (1983) 18–22.

[22] H. Gran, E. Hansen, Exchange rates of ethanol with water in water-saturated cement pastes probed by NMR, Advanced Cement Based Materials 8 (1998) 108–117.

[23] P. Sen, Time-dependent diffusion coefficient as a probe of geometry, Concepts Magn. Reson. 23A (2004) 1–21.

[24] A. L. Olsen, E. R. Washburn, Fluidities and changes in volume of the binary systems isopropyl alcohol-benzene and isopropyl alcohol-water, J. Phys. Chem. 42 (1938) 275–281.

[25] R. B. Bird, E. N. Lightfoot, W. E. Stewart, Transport Phenomena, Revised 2nd Edition, John Wiley & Sons, Inc., New York, 2007.

[26] M. Cappelezzo, C. A. Capellari, S. H. Pezzin, L. A. F. Coelho, Stokes-einstein relation for pure simple fluids, The Journal of Chemical Physics 126 (2007) 224516.

[27] J. H. Wang, Self-diffusion coefficients of water, J. Phys. Chem. 69 (1965) 4412–4412.

[28] Y. Yu, G. Gao, Study on self-diffusion in water, alcohols and hydrogen fluoride by the statistical associating fluid theory, Fluid Phase Equilibria 179 (2001) 165–179.

[29] K. C. Pratt, W. A. Wakeham, The mutual diffusion coefficient for binary mixtures of water and the isomers of propanol, Proceedings of the Royal Society of London. Series A, Mathematical and Physical Sciences 342 (1975) 401–419.

[30] F. X. Prielmeier, E. W. Lang, H.-D. Lüdemann, Pressure dependence of the self-diffusion in liquid trifluoromethane, Molecular Physics 1984 (1984) 1105–1113.

[31] R. J. Martins, M. J. E. de M. Cardoso, O. E. Barcia, Excess Gibbs free energy model for calculating the viscosity of binary liquid mixtures, Ind. Eng. Chem. Res. 39 (2000) 829–854.

[32] M. A. Barrufet, D. Dexheimer, Use of an automatic data quality control algorithm for crude oil viscosity data, Fl. Ph. Equil. 219 (2004) 113–121.

[33] D. S. Viswanath, T. Ghosh, D. H. Prasad, N. V. Dutt, K. Y. Rani, Viscosity of Liquids: Theory, Estimation, Experiment, and Data, Springer, Dordrecht, The Nertherlands, 2007.

[34] C. Yokoyama, M. Takahashi, Viscosity of CHF_3 in the critical region, International Journal of Thermophysics 18 (1997) 1369–1385.

[35] Z. Shan, S. Penoncello, R. Jacobsen, A generalized model for viscosity and thermal conductivity of trifluoromethane (R23), ASHRAE Trans. 106 (2000) 757–767.

[36] Y. Tanaka, Y. Matsuda, H. Fujiwara, H. Kubota, T. Makita, Viscosity of (water + alcohol) mixtures under high pressure, International Journal of Thermophysics 8 (1987) 147–163.

[37] J. Gross, G. W. Scherer, Dynamic pressurization: novel method for measuring fluid permeability, Journal of Non-Crystalline Solids 325 (2003) 34–47.

[38] A. R. Mahajan, S. R. Mirgane, Excess molar volumes and viscosities for the binary mixtures of n-octane, n-decane, n-dodecane, and n-tetradecane with octan-2-ol at 298.15 k, Journal of Thermodynamics 2013 (2013) 1–11.

[39] Y. Gaston-Bonhomme, P. Petrino, J. Chevalier, UNIFAC—VISCO group contribution method for predicting kinematic viscosity: extension and temperature dependence, Chemical Engineering Science 49 (1994) 1799–1806.

[40] I. Fischer, B. Pichler, E. Lach, C. Terner, E. Barraud, F. Britz, Compressive strength of cement paste as a function of loading rate: Experiments and engineering mechanics analysis, Cement and Concrete Research 58 (2014) 186–200.

[41] G. W. Scherer, Stress development during supercritical drying, Journal of Non-Crystalline Solids 145 (1992) 33–40.

[42] S. Penoncello, E. Lemmon, R. Jacobsen, Z. Shan, A fundamental equation for trifluoromethane (R-23), J. Phys. Chem. Ref. Data 32 (2003) 1473–1499.

[43] G. W. Scherer, Stress in aerogel during depressurization of autoclave: I. theory, Journal of Sol-Gel Science and Technology 3 (1994) 127–139.

[44] G. W. Scherer, J. Gross, L. W. Hrubesh, P. R. Coronado, Optimization of the rapid supercritical extraction process for aerogels, Journal of Non-Crystalline Solids 311 (2002) 259–272.

[45] A. M. Brandt, Cement-Based Composites: Materials, Mechanical Properties and Performance, Taylor & Francis, New York, 2009.

[46] Z. Zhang, Modelling of sorption hysteresis and its effect on moisture transport within cementitious materials, Ph.D. thesis, Université Paris-Est (May 2014).
URL https://tel.archives-ouvertes.fr/tel-01127302

[47] W. Vichit-Vadakan, G. Scherer, Measuring permeability and stress relaxation of young cement paste by beam-bending, Cement and Concrete Research 33 (2002) 1925–1932.

[48] Z. C. Grasley, G. W. Scherer, D. A. Lange, J. J. Valenza, Dynamic pressurization method for measuring permeability and modulus: II. cementitious materials, Materials and Structures 40 (2007) 711–721.

[49] G. W. Scherer, J. J. V. II, G. Simmons, New methods to measure liquid permeability in porous materials, Cement and Concrete Research 37 (2007) 386–397.

[50] Z. Zhang, M. Thiery, V. Baroghel-Bouny, Numerical modelling of moisture transfers with hysteresis within cementitious materials: Verification and investigation of the effects of repeated wetting–drying boundary conditions, Cement and Concrete Research 68 (2015) 10–23.

[51] Z. Zhang, M. Thiery, V. Baroghel-Bouny, Investigation of moisture transport properties of cementitious materials, Cement and Concrete Research 89 (2016) 257–268.

[52] Z. A. Kameche, F. Ghomari, A. Khelidj, M. Choinska, Measurement of the relative gas permeability of ordinary concrete: influence of saturation degree and the sample size, VIII International Conference on Fracture Mechanicsof Concrete and Concrete Structures, March 10-14,2013, Toledo, Spain, 2013.

[53] Z. Zhang, M. Thiery, V. Baroghel-Bouny, M. Nguyen, P. Rossi, Modelling of the hydration and moisture transfer coupling effects on the microstructure properties of the concrete cover, in: 2nd International conference on Microstructural-related Durability of Cementitious Composites, RILEM Publications SARL, 2012, pp. 960–968.

[54] J. M. Makar, G. W. Chan, End of the induction period in ordinary portland cement as examinedby high-resolution scanning electron microscopy, J. Am. Ceram. Soc. 91 (2008) 1292–1299.

[55] Y. F. Houst, et. al., Design and function of novel superplasticizers for more durable high performance concrete (superplast project), Cement and Concrete Research 145 (2008) 33–40.

[56] L. Tunstall, A study of surfactant interaction in cement-based systems and the role of the surfactant in frost protection, Ph.D. thesis, Princeton University (2016).

[57] L. E. Tunstall, G. W. Scherer, R. K. Prud'homme, Studying aea interaction in cement systems using tensiometry, Cement and Concrete Research 92 (2017) 29–36.

[58] Z. Zhang, G. W. Scherer, A. Bauer, Morphology of cementitious material during early hydration, Cement and Concrete Research (2017).

[59] H. M. Jennings, B. J. Dalgleish, P. L. Pratt, Morphological development of hydrating tricalcium silicate as examined by electron microscopy techniques, Journal of the American Ceramic Society 64 (1981) 567–572.

[60] P. Fonseca, H. Jennings, The effect of drying on early-age morphology of C–S–H as observed in environmental SEM, Cement and Concrete Research 40 (2010) 1673–1680.

[61] A. Bazzoni, Study of early hydration mechanisms of cement by means of electron microscopy, Ph.D. thesis, EPFL (2014).

[62] N. Yellin, L. Ben-Dor, N. Zelingher, Whisker growth by means of porous glass, Journal of Materials Science 21 (1986) 2648–2650.

[63] D. Menetrier, I. Jawed, T. S. Sun, J. Skalny, ESCA and SEM studies on early C_3S hydration, Cement and Concrete Research 9 (1979) 473–482.

[64] G. L. Kalousek, A. F. Prebus, Crystal chemistry of hydrous calcium silicates: III, morphology and other properties of tobermorite and related phases, Journal of the American Ceramic Society 41 (1958) 124–132. doi:10.1111/j.1151-2916.1958.tb13525.x.

[65] R. L. Rarick, J. J. Thomas, B. J. Christensen, H. M. Jennings, Deterioration of the nitrogen bet surface area of dried cement paste with storage time, Advanced Cement Based Materials 3 (1996) 72–75.

[66] R. Feldman, J. Beaudoin, Pretreatment of hardened cement pastes for mercury intrusion measurements, Cement and Concrete Research 21 (1991) 297–308.

[67] D.C.Hughes, The use of solvent exchange to monitor diffusion characteristics of cement pastes containing silica fume, Cement and Concrete Research 18 (1988) 321–324.

[68] D.C.Hughes, N. Crossley, Pore structure characterization of GGBS/OPC grouts using solvent techniques, Cement and Concrete Research 24 (1994) 1255–1266.

[69] J. Beaudoin, P. Gu, J. Marchand, R. Myers, Z. Liu, Solvent replacement studies of hydrated portland cement systems — the role of calcium hydroxide, Advanced Cement Based Materials 2 (1998) 56–65.

[70] NIST chemistry webbook, http://webbook.nist.gov/chemistry/, accessed: 2016-09-10.

[71] C. Rodriguez-Navarro, A. Suzuki, E. Ruiz-Agudo, Alcohol dispersions of calcium hydroxide nanoparticles for stone conservation, Langmuir 29 (2013) 11457−11470.

[72] A. B. Trenwith, Thermal decomposition of isopropanol, J. Chem. Soc., Faraday Trans. 1 71 (1975) 2405–2412.

[73] S. Niu, K. Han, C. Lu, R. Sun, Thermogravimetric analysis of the relationship among calcium magnesium acetate, calcium acetate and magnesium acetate, Applied Energy 87 (2010) 2237–2242.

[74] C. Brinker, K. Keefer, D. Schaefer, R. Assink, B.D.Kay, C. Ashley, Sol-gel transition in simple silicates II, Journal of Non-Crystalline Solids 63 (1984) 45–59.

AppendixA. Estimation of viscosity of R23/isopropanol mixture

The silica gels were made from tetraethoxysilane with the B2 recipe [74] and were cast into polystyrene pipettes (7.8 mm diameter, 10 cm long). For the corresponding aerogel, if there is no shrinkage, the relative density of gel (i.e., volume fraction of solids), ρ, is about 0.068 so the porosity is about 93% [37]. We choose silica gels because they show large strain in a pressure jump that can be accurately measured.

If a porous material endures a sudden pressure change, a spontaneous strain can be observed, because the pressure inside the body is different from that outside. In addition, there is a permanent strain ε_s, apparently resulting from the Bangham effect (i.e., a change in interfacial energy as a result of adsorption), that can be approximated by [37]

$$\varepsilon_s = \varepsilon_0 + \alpha \langle P_F \rangle \tag{A.1}$$

where ε_0 is the strain before a pressure jump, and α is a constant. The volumetric average of fluid pressure in the porous body, $\langle P_F \rangle$, is given by

$$\langle P_F(\theta) \rangle = P_A(\theta) + \int_0^\infty \phi(\theta - \theta') \frac{\mathrm{d}\Omega}{\mathrm{d}\theta'} \mathrm{d}\theta' - \left(\frac{A}{8\beta} \right) \phi(\theta) \tag{A.2}$$

where P_A is the pressure in the autoclave. A is a constant. β is a material parameter related to the Poisson ratio ν_p. The pore pressure depends on the rate of change of the function Ω, which is defined as

$$\Omega = (1 - \rho) K_p \ln \left(\frac{\rho_F(\theta)}{\rho_F(0)} \right) \tag{A.3}$$

where K_P is the bulk modulus of the porous material, $K_P = E_P/[3(1-2\nu_p)]$. E_P is the Young's modulus. θ is the reduced time, which is defined as the ratio of actual time with the hydrodynamic relaxation time $\theta = t/\tau_D$. τ_D is defined as

$$\tau_D = \frac{\beta \eta_F R^2}{k_l K_P} \tag{A.4}$$

where η_F is the viscosity of the fluid mixer. R is the radius of the gel. k_L is the permeability which depends on the microstructure of the material not on the fluid, so we can assume that the value found in [13] using CO_2 also applies for R23.

Finally, the axial strain is calculated by

$$\varepsilon_z = \langle \varepsilon_s \rangle + \frac{\langle P_F \rangle - P_A}{3K_P} \tag{A.5}$$

Equation A.5 was used to fit the measured strain with the only unknown parameter being η_F. All other parameters for the silica gel are taken from [37].

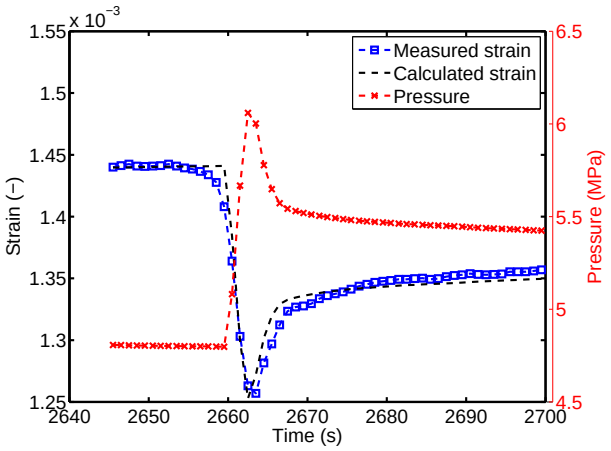

Figure A.23: Fitted pressure-strain curve.

In a test, a 7-cm long silica gel was immersed in 300 mL isopropanol in the extractor (see Fig. 11). After pressure increases until R23 turns into liquid, the test can start. An example with both measured and fitted curves is shown in Fig. A.23. The fitted viscosities for isopropanol/R23 mixtures are given in Table 3. When the extractor is filled with the pressurized liquid R23, the isopropanol mole fraction is about 0.3 as indicated in Table 3 as well.